HHS Public Access

Author manuscript

RSC Adv. Author manuscript; available in PMC 2018 August 29.

Published in final edited form as:

RSC Adv. 2015 ; 5(112): 92189–92206. doi:10.1039/c5ra19106h.

Synthesis and characterization of Co/Ti layered double hydroxide and its application as a photocatalyst for degradation of aqueous Congo Red†

Priyadarshi Roy Chowdhury and **Krishna G. Bhattacharyya***

Department of Chemistry, Gauhati University, Guwahati-781014, Assam, India.

Abstract

2 : 1 Co/Ti layered double hydroxide (LDH) was synthesized hydrothermally using commercially available $Co(NO_3)_2{\cdot}6H_2O$ and $TiCl_4$, on a urea template. The high surface area material (~180 m^2 g^{-1}) had a narrow band gap (2.67 eV) and shallow and deep trap defect sites. The layered nanomaterial exhibited remarkable semiconductor properties and demonstrated excellent visible light decolourisation efficiency for the anionic dye Congo Red in aqueous medium. The photocatalytic efficiency of the LDH was better than common commercial materials in use such as ZnO, ZnS, NiO, CoO, TiO_2 and Degussa P25. The presence of different surface states of defect sites in the LDH was confirmed by PL, EIS and XPS measurements. XRD, DRS, FT-IR, AFM, TEM, SEM/EDX and TG/DTG analyses yielded information about the structural, morphological properties and thermal stability of the LDH. BET N_2 adsorption-desorption measurements at 77 K gave surface area and porosity data for the LDH. The surface charge characteristics of the LDH were evaluated with ξ-potential measurements over a wide pH-range in aqueous medium. The photocatalytic behaviour towards decolourisation of the dye was evaluated depending on the reaction variables of pH, LDH amount, initial dye concentration and effects of quenchers, and variation of molar ratios of Co/Ti LDH. The pseudo-first order model satisfactorily described the degradation kinetics of the anionic dye. The photocatalytic mechanistic pathways of the LDH were explained on the basis of an electron-hole (e^--h^+) hopping conduction model and also photosensitization of the dye. The maximum catalytic efficiency was observed with 15.0 mg of LDH at pH 4 for the anionic Congo Red dye at a concentration 1×10^{-5} M. The LDH was stable even after the fifth catalytic cycle, indicating its remarkable efficiency in potential decolourisation treatments. The dye degradation products were analysed with GC-MS and a reaction mechanism was proposed for the breakdown of the dye to simple and less toxic components.

1. Introduction

The search for suitable semiconductor photocatalysts for wastewater remediation is one of the most important aspects of environmental science. Light assisted degradation of carcinogenic and neurotoxic dyes present in industrial effluents by photocatalysts is a complicated task, since it occurs through several photon-initiated redox reactions.

†Electronic supplementary information (ESI) available: Characterization and photoassisted degradation results associated with this work.

kgbhattacharyya@gmail.com; Fax: +91 3612570599; Tel: +91 9864031987.

Conventional photo-catalytic systems employing TiO_2, have been extensively investigated, but the considerably large band gap of TiO_2 (>3 eV) limits its use under UV irradiation only. The introduction of suitable dopants has been shown to be very effective towards extending the photocatalytic activity of TiO_2 into the visible light region. However, as the dopants act as recombination centres of charge carriers, the photocatalytic efficiency decreases. In order to overcome this limitation, recent approaches are centred on the creation of Ti^{3+} centres by narrowing the band gap.

Layered double hydroxides (LDHs) constitute a large family of anionic clay materials possessing 2D inorganic layered matrices and have the general formula, $[M^{II}_{1-x}M^{III}_{x}(OH)_2]-(A^{n-})_{x/n}\cdot yH_2O$, where M^{II}, M^{III} represent divalent, trivalent cations respectively and A^{n-} is the charge balancing anion present in the interlayer. The LDH layers are brucite-like containing divalent metal cations (Mg^{2+}, Fe^{2+}, Co^{2+}, Ni^{2+}, Zn^{2+}, *etc.)* in octahedral positions coordinated to the hydroxyl groups. The divalent cations can be substituted isomorphously with triva-lent cations (Al^{3+}, Cr^{3+}, Ga^{3+}, In^{3+}, Mn^{3+}, Ti^{3+}, Fe^{3+}, *etc.)* creating positively charged layers. Water molecules and inorganic or organic charge-compensating exchangeable anions occupy the interlayer galleries. The hydroxyl groups are oriented towards the interlayer region or may be hydrogen bonded to the inter-layer anions as well as to water molecules. LDH materials possess weak interlayer bonding due to which they exhibit excellent properties of expansion. The LDHs have found use as polymer fillers[1–3] and as novel materials with unique magnetic,[4–6] catalytic and photochemical functions[7] due to their structural and compositional variability. The LDH could be converted to the corresponding mixed metal oxide, $M^{II}M^{III}_2O_4$ by heating.[8] The LDH decomposition is extensively employed in designing oxide and oxide-supported catalysts.

In recent times, attention has been increasingly focused towards the development of novel and efficient photocatalysts for application in the field of environmental management. Important considerations in the different approaches have been low cost, stability and large scale applicability in redox processes. The LDH-based composite photocatalysts have been extensively tested in a number of redox reactions, including photocatalytic degradation of organic pollutants and selective organic transformations.[9]

In the present work, 2 : 1 Co/Ti LDH was synthesized on urea template, characterized with a number of physical, chemical and spectroscopic techniques and was tried as a photocatalyst for the degradation of the anionic dye, Congo Red in water. Congo Red is extensively used in printing, textile and photographic industries[8–10] and is a component of the coloured effluent discharged by such industries. This work tries to destroy the dye through photochemical reaction over 2 : 1 Co/Ti LDH in aqueous medium using visible light as the energy source.

2. Experimental section

2.1. Materials

All analytical grade chemicals were purchased from Merck Chemicals, USA and were used without further purification. De-ionized and decarbonated water was extensively used throughout the experiments.

2.2. LDH synthesis

$Co(NO_3)_2 \cdot 6H_2O$, $TiCl_4$ and urea were used for synthesizing 2 : 1 Co/Ti-LDH using co-precipitation method from a homogenous solution. In the typical synthesis, 11.78 g of $Co(NO_3)_2 \cdot 6H_20$, 1.1 ml $TiCl_4$ and 3.0 g of urea, were dissolved in 100 ml decarbonated water at room temperature (~30 xC) and the contents were vigorously stirred for 3 h. The mixture was allowed to age in Teflon lined autoclave at 140 °C for 36 h and the dark pink crystalline product was extracted by centrifugation, washed several times with de-ionized water and dried at 100 xC for 4 h. The product was designated as 2 : 1 Co/Ti LDH.

2.3. Preparation of Congo Red solution

The stock solution of the anionic Congo Red (CR) (Fig. 1) of 1.0×10^{-3} M [=619.66 mg L^{-1} of CR] was prepared by dissolving its accurate amount in de-ionized water. The stock solution was diluted further to obtain the experimental solutions of 1.0×10^{-4} and 1.0×10^{-5} M respectively to be used for degradation reactions.

2.4. Characterization of the LDH

X-ray diffraction (XRD) pattern was recorded using a PANalytical X'Pert PRO diffractometer that allowed reflection as well as transmission mode measurements. Reflection mode experiments were performed with a conventional Bragg-Brentano geometry. The incident CuK_α X-ray beam (40 kV; 30 mA) was passed through a 0.02 rad Soller slit, a 1/8 divergence slit, a 15 mm fixed mask, having a 1/4 anti-scatter slit. The diffracted beam was detected with a PIXcel linear sensitive detector possessing β filter, a 0.02 rad Soller slit and a 1/8 anti-scatter slit. The diffraction patterns were recorded in 2θ range of 5–80° with step size of 0.013° and acquisition time of 15 s per step. The transmission-mode data was recorded using an elliptic focusing mirror, 0.5° divergence slit, 0.5° anti-scatter slit and 0.02 rad Soller slit in the primary beam.

FT-IR measurements were performed with a Shimadzu FT-IR 3000 spectrometer (resolution 4 cm^{-1}); the sample was mixed with KBr in the weight ratio of 1 : 100 and was pressed into a disc.

Thermogravimetric analysis (TG) from 32 to 750 °C was done in a Mettler Toledo Thermal Analyser in an inert atmosphere with a heating rate of 10 °C min^{-1}.

Brunauer-Emmett-Teller (BET) N_2-adsorption method (Micromeritics TriStar 3000 V6.08 analyzer) along with Barrett-Joyner-Halenda (BJH) computation procedure was used to obtain specific surface area, pore volume and pore size. Co/Ti-LDH sample was degassed at 120 °C for 3 h before analysis.

The electrochemical impedance spectroscopy (EIS) analysis of the Co/Ti LDH was conducted with CHI 760E Chenhua Instruments (Shanghai) electrochemical workstation in a conventional three-electrode cell having Pt wire as the counter electrode, saturated calomel electrode as the reference electrode and LDH deposited on ITO glass as the working electrode. 0.5 M Na_2SO_4 solution was taken as the electrolyte.

The X-ray photoelectron spectroscopy (XPS) surface survey of 2 : 1 Co/Ti-LDH was taken with PHI Quantum 5800 ESCA instrument, equipped with micro-focussing, monochromatic Al-K_α as the X-ray source. UV-vis diffuse reflectance spectra (DRS) of LDH were obtained with Hitachi U4100 spectrometer on $BaSO_4$ background. The morphology of 2 : 1 Co/Ti LDH was examined with Zeiss Supra 55 scanning electron microscope (SEM) with an accelerating voltage of 20 kV. The layered structure was investigated using a Philips TECNAI-20 and JEOL JEM-2010 high resolution transmission electron microscope with accelerating voltage of 200 kV. The elemental composition was determined with Oxford INCA EDX 300 microanalysis attachment associated with the SEM instrument. The morphology and the LDH layers were investigated with atomic force microscopy (AFM) in the tapping mode (Cypher S atomic force microscope, Asylum Research, Oxford Instruments). The sample was prepared on 4×4 cm^2 mica plate. A Si tip with 10 nm radius (Mikromasch) was used to record high resolution micrographs. Height-mode images were recorded simultaneously with 512×512 pixels at the scan rate of 1–2 Hz.

The electrical properties of the LDH surface in aqueous medium were determined with a Malvern Zetasizer Nano ZS instrument in the pH range of 4–11.

Photoluminescence (PL) spectra were obtained at different excitation wavelengths in a fluorescence spectrometer (Hitachi F-2500 FL spectrophotometer) with a Xe-lamp as the excitation source. The absorption spectra of the dyes were monitored with Shimadzu 1800 UV-vis spectrometer. The decolorized end products of photodegradation were identified by GC/MS (Varian 3900GC-Saturn 2100T) with column temperature programmed as 40 °C (1 min), 40–200 xC (7 °C m in^{-1}, hold time: 5 min).

2.5. Photocatalytic reactions

The photo-assisted dye degradation experiments were carried out in a visible light photocatalytic reactor (Fig. 2) comprising of a stainless steel chamber fitted with a 300 W tungsten lamp (Philips 38941–1; PS25, Frost-6100) as the visible-light source and a wavelength pass filter ($\lambda > 400$ nm) beneath the chamber. Prior to visible light irradiation, the reactants were stirred vigorously for 30 min in dark to establish adsorption/desorption equilibrium between the catalyst and the dye. The degradation of the test dye, Congo Red was investigated in aqueous solution at 30 °C (room temperature) with continuous circulation of running water through the outer jacket of the reactor ensuring constant temperature. At each 15 min interval, 10 ml aliquots were taken out, centrifuged to remove solid LDH particles and the centrifugate was analyzed for unconverted CR dye using Shimadzu UV-1800 spectrophotometer at λ_{max} value of 497 nm for aqueous CR.

Blank (without catalyst) and dark reactions were carried out following the same procedure. The effects of pH on photo-assisted degradation were investigated from pH 4.0 to 11.0 by addition of either HCl or NaOH (0.1 M). The effects of LDH amount were studied with loadings of 5.0, 10.0, 15.0 and 20.0 mg in 200 ml dye solution (1.0×10^{-5} M) at pH 4.0 (optimum pH). In another set of experiments, initial dye concentrations of 1.0×10^{-3}, 1.0×10^{-4} and 1.0×10^{-5} M were taken with fixed LDH loading of 15.0 mg in 200 ml of dye solution. The photo-catalytic effects were also investigated by varying the molar concentration of Co and Ti in the LDH under optimum conditions. For comparison of the

performance of 2 : 1 Co/Ti LDH, CR photodegradation was carried out with commercial ZnO, ZnS, NiO, CoO, TiO_2 and Degussa P25 photocatalysts (15.0 mg of catalyst in 200 ml of 1.0×10^{-5} M Congo Red solution).

The degradation kinetics was evaluated under optimum conditions (dye concentration = 1.0×10^{-5} M, pH = 4, catalyst 15.0 mg/200 ml, temperature 30 °C). To study the role of quenchers, Na-EDTA (h^+ scavenger), n-butanol ($^{\bullet}OH$ scavenger), and benzoquinone ($O_2^{\bullet-}$ scavenger) were added to the dye solution at the beginning of the degradation experiments. The photostability of the LDH was evaluated by comparative FT-IR analysis of the pure LDH and the LDH recovered after a fifth catalytic cycle.

3. Results and discussion

3.1. X-ray diffraction analysis

The X-ray diffraction pattern of the synthesized LDH (Fig. 3) shows characteristic Bragg reflections from the hexagonal LDH phase with interlayer CO_3^{2-} ions, similar to the previously reported X-ray diffraction data for LDHs.

The diffractogram showed the existence of well-defined series of (00*l*) Bragg reflections indicating the presence of parallel layered house-of cards type stacking of Co/Ti LDH crystallites. The presence of (003), (006) and (009) reflections at 2θ values of 11.49°, 22.98° and 34.47° respectively indicates intercalation of CO_3^{2-} ions and H_2O molecules within the LDH lattice,[2,6] while the (100) XRD peak was observed at 32.31° (2θ). The *d*-spacing corresponding to the (003) peak was 0.763 nm ($2\theta \approx 11.49°$) and that of (110) was 0.146 nm ($2\theta \approx 28.35°$). These are in good agreement with previously reported data for Ti-LDHs with interlayer CO_3^{2-} anions.[8,11–15] Since the basal spacing of the synthesized 2 : 1 Co/Ti LDH is similar to that of the normal LDHs, it is most likely that the planar orientation of the interlayer CO_3^{2-} and H_2O molecules has retained a similar pattern. Moreover (110) and (101) peaks at 2θ values of 28.35° and 37.44° indicate the existence of the anatase phase of TiO_2 in the layered nanomaterial. The diffraction peaks at (018), (01$\underline{11}$), (113) and (10$\underline{13}$) at 2θ values of 47.12°, 53.35°, 67.61° and 76.58° respectively could also be indexed to typical LDHs. The presence of narrow and sharp diffraction peaks represents good crystallinity.[2,3] The XRD lattice parameters are illustrated in Tables S1 and S2; (ESI†).[12,16–18]

3.2. X-ray photoelectron spectroscopy analysis

X-ray photoelectron spectroscopy (XPS) is employed to have a well-established surface survey of the LDH and the results are presented in Fig. 4(A-G). The chemical states of the elements were identified by comparing the photoelectron binding energies (BE) of the ones reported in the literature. The XPS survey spectrum identifies the presence of elements in their respective oxidation states on the surface of the Co/Ti-LDH which is accompanied by oxygen vacancies. Fig. 4(A) shows the photo-electron lines at binding energies of 198, 289, 403, 455.4, 529 and ~780–805 eV which could be attributed to Cl2p, C1s, N1s, Ti2p, O1s and Co2p respectively. The high resolution Ti2p XPS spectrum of Co/Ti-LDH [Fig. 4(B)]

†Electronic supplementary information (ESI) available: Characterization and photoassisted degradation results associated with this work.

indicates two asymmetric peaks at binding energies of 455.4 eV and 462.7 eV corresponding to $Ti2p_{3/2}$ and $Ti2p_{1/2}$ spin states. Thus, the LDH surface shows the presence of two titanium species. Apart from the contributions from Ti^{4+} species, shoulders associated with $Ti2p_{3/2}$ and $Ti2p_{1/2}$ peaks at binding energies of 457.6 eV and 464.7 eV respectively could be attributed to Ti^{3+}, as observed in previous reports.[19–24] The surface reduction of Ti indicates the existence of negatively charged oxygen vacancies on the surface, the negative charge being shared by Ti cations adjacent to the defect sites.

Co2p XPS spectra yielded four peaks [Fig. 4(C)]. Two sharp peaks were observed at 780.4 eV and 795.9 eV corresponding to the spin states, $Co2p_{3/2}$ and $Co2p_{1/2}$ respectively. The peak splitting between the two states was $\Delta E = 15.5$ eV, representing Co^{2+} and Co^{3+} in their respective oxide phases. The weak satellite peaks at 785.3 eV and 805.2 eV also support the existence of Co in two oxidation states on the LDH surface.

Cl2p XPS line [Fig. 4(D)] indicates the presence of a strong photoelectron peak at 198.3 eV representing $2p_{3/2}$ spin state of Cl and a satellite at 199.5 eV. Their presence indicates that Cl^{-}ions are physisorbed on the LDH surface. The occurrence of Cl^{-} is due to the use of $TiCl_4$ as a precursor of Ti in synthesizing Co/Ti-LDH.

The positions of the carbon components could be correlated with the high resolution C1s spectrum of the synthesized LDH [Fig. 4(E)] and it is established that the peak corresponding to the binding energy of 289.3 eV is due to the presence of CO_3^{2-} species in the interlayer gallery of Co/Ti-LDH. C and N peaks are observed in the XPS spectra due to the use of urea and Conitrate salts in synthesizing Co/Ti LDH.

N1s line [Fig. 4(F)] shows two XPS peaks at binding energies of 403.2 eV and 405 eV respectively. The binding energy associated with the N1s line is very sensitive to the chemical environment and varies from 396 eV to 408 eV. The X-ray photoelectron peak at 403.2 eV is associated with the terminally bonded well screened molecular nitrogen (γ-N2) and that at 405 eV could be attributed to the terminally bonded poorly screened molecular nitrogen (γ-N_2) species. Thus the spectroscopic features of N1s XPS line showed striking similarity with the chemisorbed states of N_2 as illustrated in the previous reports.26 Meanwhile, the peak at 408 eV arises due to the presence of NO_3^{-} as an impurity on the surface of 2 : 1 Co/Ti-LDH, which originated as a result of utilizing hydrated cobalt nitrate as a precursor of cobalt in synthesizing the LDH.[24,25]

O1s line reveals two peaks – O_I and O_{II} representing the two different types of oxygen species on the LDH surface [Fig. 4(G)]. This is found to be in accordance with the previous reports that O_I with a lower BE of 529.4 eV is most likely to be the lattice oxygen bound to metal cations in the LDH, whereas O_{II} having higher BE of 530.9 eV could most likely belong to surface oxygen species, including mainly the oxygen species of hydroxyl groups.[19]

3.3. Electrochemical impedance spectroscopy analysis

The electrochemical impedance spectroscopy (EIS) analysis of the Co/Ti LDH was carried out to investigate the charge transfer resistance and the separation efficiency between the

photo-generated electrons and holes. The impedance analysis was done using 2.5 mM $K_3[Fe(CN)_6]/K_4[Fe(CN)_6]$ (1 : 1) mixture in 0.5 M Na_2SO_4 aqueous solution as the redox probe. The arc radius of the impedance spectrum reflects the interface layer resistance arising from the LDH electrode surface. Smaller arc radius infers higher charge transfer efficiency of the material. In case of the synthesized LDH, a small arc radius was observed in the electrochemical Nyquist plot [Fig. 7(A)], suggesting that interfacial charge-transfer could occur easily and rapid transport of charge carriers could be achieved with an effective charge separation facilitating the semiconduction mechanism. Thus, the overall electron transporting properties of 2 : 1 Co/Ti LDH could be associated with the suppression of e^-–h^+ pair recombination, which is supported by photoluminescence results, leading to the highly efficient photoassisted degradation of dyestuffs.[9]

In order to investigate the electronic properties associated with the synthesized Co/Ti LDH, Mott-Schottky (MS) measurements were performed using the impedance technique and the results are shown in [Fig. 7(B)]. The consistency in the reverse sigmoid nature of the MS plot of 2 : 1 Co/Ti LDH electrode signifies its n-type semiconductor properties. The flat band potential (V_{fb}) could be obtained from the *x*-intercept of the linear region of the MS plot. The negative V_{fb} (–0.79 V *vs.* SCE; equivalent to −0.54 *vs.* NHE) suggests the presence of different surface states of metals which could lead to considerable changes in the band positions. The phenomenon of the presence of negative flat band and the presence of different surface states is illustrated on the basis of Fermi-level pinning. Surface states occurring at the semiconductor-liquid interface, play an important role in the performance of the photoelectrochemical devices. In the absence of a redox couple, the flat band potential (V_{fb}) corresponds close to the energy of the conduction band edge (E_c) in an n-type semiconductor (Fig. 5).

At V_{fb}, in absence of specific adsorption, the potential drops across the Helmholtz layer, $\Delta\varphi_H$, which corresponds to the potential attributable to the dipoles oriented at the interface, V_d, while the potential at the space charge region of the semiconductor, $\Delta\varphi_{SC}$, is zero. In the impedance measurements, a reasonably concentrated electrolyte has been used so that the potential drop across the diffuse double layer could be neglected. If the potential difference between the semiconductor LDH surface and the solution is varied by application of an external potential (located at $E_{redox} = eV_{redox}$), $\Delta\varphi_H$ remains unchanged, while $\Delta\varphi_{sc}$, remains equal to the applied potential (assuming no specific adsorption of redox couple and no change in V_d). This forms the basis of the usual model in which the band energies are said to have remained fixed [*i.e.* $\Delta(\Delta\varphi_H) \approx 0$] and under these conditions, the open circuit photopotential (ΔV) is represented by the equation

$$\Delta V = \left| V_{fb}^0 - V_{redox} \right| \quad (1)$$

For couples with energies outside the band gap, no photo-response is expected. Eqn (1) forms the basis of selection of redox couples with potentials corresponding to energies near the valence band edge (for n-type semiconductor) in order to maximize the output photovoltage of a photoelectrochemical cell. The flat band potential, however, shifts by

specific adsorption of ions, since the potential drop across the Helmholtz layer in presence of the surface charge, q_s, is given by eqn (2)

$$\Delta\varphi_H = \frac{q_s}{C_H} + V_d = \frac{q_s}{\varepsilon\varepsilon_0/d} + V_d \quad (2)$$

where C_H is the Helmholtz layer capacitance, ε is the dielectric constant, ε_0 is the permittivity of free space and d is the thickness of the Helmholtz layer. Thus, adsorption of anions ($q_s < 0$) will cause a negative shift in the V_{fb}, which has been exactly observed in case of Co/Ti LDH. Since surface states are present in the Co/Ti LDH, they may be filled or emptied either by interaction with the solution redox couples, or by photoprocess or charge redistribution within the semiconductor LDH material. The overall effects of filling or emptying of the surface states result in the generation of surface charge, which is a function of the number of states and their respective occupancies. According to eqn (2), V_{fb} will shift producing a relative location of the conduction and valence band edges with respect to solution redox-couple energy level. Since the surface state density is large in the LDH, a potential change between the semiconductor LDH material and the solution will result in an almost equal change in $\Delta\varphi_H$ (with $\Delta\varphi_{sc}$ remaining constant). Under these conditions, Fermi level is pinned to the energy level of the surface states (E_{ss}) and the photopotential becomes independent of Vredox (Fig. 6). When Fermi-level pinning exists, photoelectrochemical effects may be observed for couples whose redox potentials are apparently located outside the gap region (depending on V_{fb}^0 value). Thus, the surface charge on the Co/Ti LDH electrode shifts in the flat band position resulting in Fermi-level pinning.[26]

The existence of different oxidation states in Co/Ti-LDH is in accordance with the XPS results. Moreover, Co has excellent electrochemical properties owing to its electronic configuration. Therefore, the rapid transport of charge carriers with an effective charge separation could be easily achieved. The overall transport properties of the LDH could be attributed to the suppression of charge recombination, which contributes to its high rate of photocatalytic performance.

On the basis of the impedance results, the enhanced photocatalytic behaviour of the Co/Ti LDH could be attributed to the separation of charge carriers, extended photo responding range, the negative flat-band potential accompanied by higher migration efficiency of photo induced electrons. The conduction band potential (E_{CB}) of n-type semiconductor ranges from 0 to −0.2 V; very close to the V_{fb} obtained for 2 : 1 Co/Ti-LDH, and is dependent on the effective electronic mass and carrier concentration. In this measurement, the voltage difference between the conduction band and the flat band potential is fixed at 0.1 V. Thus the negative value of Fermi level in the Co/Ti LDH electrode causes E_{CB} to lie at −0.54 V *vs.* NHE. The conduction band potential, so obtained for the LDH indicates a stronger reductive power, which may be effectively involved in the oxygen reduction reaction. As the standard redox potential of $O_2/O_2^{\bullet-}$ (–0.28 V *vs.* NHE) is more positive than E_{CB} measured for the LDH, it suggests that the photo-generated electrons could theoretically react readily with the adsorbed O_2 toform $O_2^{\bullet-}$ on Co/Ti LDH surface. Thus, Co/Ti-LDH could efficiently transfer

photo-generated electrons from the surface leaving more h^+-type charge carriers that assist in the photo-degradation of dyestuffs in aqueous medium.

3.4. Photoluminescence analysis

Photoluminescence technique (PL) is employed to understand the fate of e^-–h^+ pairs in the LDH as well as to examine the mechanism of trapping, migration and transfer of charge carriers [Fig. 8(A)]. Photoluminescence emissions that usually give a better understanding of the optical properties, surface states and defect sites, are broadly divided into two categories: the band-band PL emissions due to electronic transitions from the conduction band (CB) bottom to the valence band (VB) top and excitonic PL emissions resulting from the surface oxygen vacancies and other defects present in the semiconductors. For band-band PL emissions, the lower the intensity, higher is the separation rate of photo-induced electron-hole [(e_{CB}^-)-(h_{VB}^+)] pair and higher is the photocatalytic activity.[9,27] In case of excitonic emissions, the relationship between the luminescence intensity and photocatalytic activity is quite complicated and depends on the electronic properties of semiconducting materials.

The ultraviolet emission analysis of Co/Ti LDH was carried out under excitation wavelengths of 390 nm, 400 nm and 410 nm respectively. It is seen that the intensity decreased on increasing the excitation wavelength, which is attributed to higher separation of the charge carriers. The higher separation of charge carriers reflects the consistency with the results of electrochemical impedance measurements. Studies have suggested that oxygen vacancies along with surface defects bind the photo-induced electrons forming excitons, so that the PL signal can easily occur. Moreover, Ti doped photocatalytic systems consist of two kinds of trap sites for holes, the deep hole and the shallow hole. The deep trapped holes exhibit lower oxidizing potential, prefer to undergo reaction with physisorbed substances.

The synthesized LDH showed several excitonic PL emissions at 432 nm (2.87 eV), 463 nm (2.67 eV), 472 nm (2.63 eV), 511 nm (2.43 eV), 534 nm (2.32 eV), 563 nm (2.2 eV), 573 nm (2.16 eV), accompanied by a valley extending up to 633 nm, resulting from the oxygen vacancies associated with the surface and defects within the LDH, which has led to a significant enhancement in its optical properties. The emission peak at 463 nm (2.67 eV) is attributed to the exciton from conduction band (e_{CB}^-) to valence band (h_{VB}^+), equal to the band gap energy of the synthesized Co/Ti LDH nanomaterial (determined from Tauc plot analysis). Apart from this peak, the other emission peaks are mostly associated with excitons as well as oxygen defect related shallow and deep trap centers. The emission at 432 nm is observed due to self-trapped exciton (STE), generated on the LDH lattice due to hole capture by a trapped electron. The STE is of two types, direct and indirect. The direct STE emission is caused by the direct recombination of the charge carriers, while indirect STE emission is caused by recombination *via* an oxygen vacancy. Since Ti doping generates oxygen vacancy, the STE emission at 432 nm is assumed to be formed *via* oxygen vacancies and is of indirect nature.[36] The emission peaks at 472, 534, 563 and 573 nm are due tof or F^{2+} and F^+ color centers respectively. An F-center is the oxygen vacancy with two trapped electrons; F^+ is with a singly trapped electron whereas F^{2+} is the oxygen vacancy with no trapped electrons. The oxygen defects associated with these emissions occur due to oxygen vacancies in the shallow and deep level in the band gap of LDH. The absorption peaks

associated with the oxygen defects are in the range of 450–630 nm, therefore the emission peaks in the luminescence spectrum of the LDH are certainly associated with different types of charged (F, F^+ or F^{2+}) oxygen vacancy states and are of deep trap emissions in nature. On the other hand, the emission peaks below 450 nm are shallow trap emissions. The oxygen defects associated with the grain boundary are distributed randomly, are charged (F, F^+ or F^{2+}) and act as shallow trap centers. In addition, lattice site oxygen defects, forming deep trap centers, are also charged. The free electrons, not trapped in these defects migrate throughout the lattice and recombine with the holes inside or on the surface of the LDH. But the migrating electrons are strongly repelled by the charged oxygen vacancy sites and are not easily allowed to recombine with the holes. Since the existence of defect states originate due to doping, the mobility of carriers is slowed down, which delays the recombination process.

The dopants present on the LDH surface act as an obstacle to efficient overlapping of carriers on the surface. The defect sites act as active trap centers and separate the charge carriers. Doping also shifts the band edges and the conduction band electrons have to traverse an indirect path for undergoing recombination with the holes. This delays the recombination and quenches the emission intensity. Since the emission intensity is reduced with an increase in excitation wavelength, the quenching effect is expected to play an important role. In conformity with this, doping increases the interaction among dopant and defects and form quenching centers. The electrons are first captured by shallow trap levels, and then they jump to Co or Ti d-states, which further jump from one d-state to another and thus, form some quenching centers. The electrons, after passing through a channel of dopant and defects, ultimately find a recombination center and emit light. But, this process increases the time period for the charge carriers to undergo recombination and therefore a reduction in the emission intensity is observed. Thus, the presence of defects within the microstructures of the synthesized LDH is expected to play a major role in its highly efficient photocatalytic performance.

3.4.1. Mechanism of photoluminescence emission—Depending on the UV-emission peaks of the LDH in aqueous medium, a mechanism has been suggested and is schematically illustrated in Fig. 8(B). On exciting the LDH at 390, 400 and 410 nm respectively, the electrons jump from the valence band (VB) to the upper region of the conduction band (CB) and thereby fall to its bottom without emission of photon (step 1). From the bottom of CB, a few electrons may emit UV light (step 2) whereas some of them jump further to the shallow trap centers and then undergo photon emission (step 3). The deep trap centers are filled up progressively with the electrons coming from shallow trap centers. The electrons from deep trap centers may also directlyjump to the valence band (step 4) or jum p to the d-states of the metals and recombine with the valence band holes (step 5). The semiconductor, Co/Ti LDH, possessing defects within its layered microstructures, therefore facilitates the photoassisted degradation.

3.5. Zeta potential measurements

The variation of the surface charge of aqueous Co/Ti-LDH with pH was monitored with zeta potential measurements from pH 4–11 (Fig. S1; ESI†). The pH was adjusted by adding

drops of 0.1 M HCl or NaOH to the aqueous LDH solution. It was observed that the surface charge of the LDH decreased monotonically with the increase in pH, attaining zero point charge (zpc) at pH 7.44, the iso-electric point of the LDH.[28,29] Thus, Co/Ti-LDH surface attains positive charge at pH < pH_{zpc}, attracting negatively charged Congo Red anions in aqueous solution, enabling a higher photodegradation efficiency. The maximum photo-catalytic degradation was observed at the pH 4, when the LDH surface is sufficiently positive.

3.6. BET/BJH-N2 sorption analysis

The low temperature N_2-sorption analysis in an inert atmosphere showed a type IV isotherm with a considerably large H3-type of hysteresis loop (p/p_0 > 0.4–0.8) for the Co/Ti LDH [Fig. S2(A); ESI†]. The large hysteresis loop indicates the condensation of N_2 inside the pores of the LDH. In the desorption phase, the gas is released through a different path with reduction in the pressure, a property shown by the mesoporous materials.[8,11] Thus, 2 : 1 Co/Ti LDH consists of mesopores formed by the accumulation of particles. The comparatively broad average pore width of 3.91 nm in 2 : 1 Co/Ti LDH is most likely to have originated due to use of urea as the template during the hydrothermal synthesis [Fig. S2(B); ESI†]. The high BET specific surface area of 180 $m^2\ g^{-1}$ and the BJH adsorption and desorption cumulative pore volumes of 0.246 and 0.218 $cm^3\ g^{-1}$ respectively for Co/Ti-LDH indicate the suitability of the material as a catalyst. The LDH is dominated by micro- and mesopores of 1 to 6 nm diameter. The meso-porous character of the material with appropriate spatial arrangement of the pores is likely to assist in e^--h^+ transfer within the LDH framework resulting in high photocatalytic performance.[8]

3.7. FT-IR analysis

The FT-IR spectrum of the 2 : 1 Co/Ti LDH (Fig. S3; ESI†) showed the characteristic frequencies associated with the layered structure having interlayer CO_3^{2-} ions and H_2O molecules. The intense and strong absorption band centered on 3435 cm^{-1} could be attributed to stretching vibrations of surface and interlayer water molecules and hydroxyl groups. The lower frequency in Co/Ti LDH compared to normal OH_{str} vibration of free water at 3600 cm^{-1}, indicates the presence of H_2O molecules in the interlayer gallery of the LDH. This could also be due to the formation of hydrogen bonds associated with interlayer water with guest anions and hydroxide groups of the intrinsic layers.[8] The band at 3173 cm^{-1} accompanied by a hump near 2932 cm^{-1} could also be attributed to hydrogen bonding between the interlayer H_2O and CO_3^{2-} ions. The band at 1635 cm^{-1} is assigned to bending vibrations of H_2O molecules. In most hydrotalcites, three IR active absorption bands arising from CO_3^{2-} species are observed at 1408 cm^{-1} (ν_3), 1125 cm^{-1} (ν_1) and 714 cm^{-1} (ν_2). The band at 1408 cm^{-1} is attributed to ν_3 mode of interlayer CO_3^{2-} species of the LDH.[8] The band at 862 cm^{-1} is observed due to metal-hydroxyl (M-OH) groups present in the lattice of the LDH.[17,18] The 622 cm^{-1} sharp band is associated with in-plane quadrant bending and that of 714 cm^{-1} could be attributed to ν_2 mode of CO_3^{2-} species. The occurrence of the three characteristic bands in the LDH synthesized in the present work, along with the XRD data, confirms successful incorporation of CO_3^{2-} and H_2O molecules in the interlayer gallery of the Co/Ti LDH.

3.8. UV-visible DRS analysis

The UV-vis diffuse reflectance spectroscopy analysis is performed to determine the electronic properties of the Co/Ti LDH [Fig. 9(A)]. The DRS investigated the nature and coordination state of Co and Ti within the layered material. The hump at ~260 nm is attributed to d-d transitions. The strong absorption band around 320 nm could be assigned to typical $Co_{(II)}$ coordinated to the CO_3^{2-} anions present in the interlayer galleries.[1,8,21] The broad absorption band from ~410–700 nm is observed with a maximum at ~548 nm indicating the presence of Ti^{4+} in the brucite like sheets. It also signifies guest-guest or guest-host supramolecular interactions. In comparison to the commercial catalysts, Co/Ti LDH showed an overall band broadening accompanied by a red shift in the UV-visible absorption spectrum, which is most likely to be due to the formation of aggregates.[8]

3.8.1. Comparative study of optical properties of the catalysts.—The comparative study of the UV-vis DRS of 2 : 1 Co/Ti-LDH with a few important commercial catalysts like ZnO, ZnS, CoO, TiO_2, NiO and Degussa P25 [Fig. 9(A)] showed strong absorbance at ~260–450 nm for all the catalysts, with a minor shift in λ_{max} position for the synthesized Co/Ti LDH. Moreover, Co/Ti-LDH also exhibited broad absorption between 410–700 nm, which was not observed in any of the other commercial catalysts. The strong absorbance in the visible region makes the LDH, a highly efficient photocatalyst compared to commercial ZnO, ZnS, CoO, TiO_2, NiO and Degussa P25. UV-vis absorption analysis is considered to be very convenient and effective for explaining the band structure of semiconductor materials. The band gap of LDH along with that of the commercial catalysts was calculated from solid UV-visible diffuse reflectance study [Fig. 9(B)] using the Tauc equation[21]

$$\varepsilon h\nu = C\left(h\nu - E_g\right)^n \quad (3)$$

where, E_g represents the optical band gap, $h\nu$ is the photon energy, ε is the molar extinction coefficient, C is a proportionality constant and n has the values of 1/2, 3/2, 2, and 3 for direct allowed, direct forbidden, indirect allowed and indirect forbidden transitions respectively. In case of 2 : 1 Co/Ti LDH, the best fit of $(\varepsilon h\nu)^2$ *vs.* $h\nu$ was obtained for n = 1/2, suggesting a direct allowed electronic transition across the energy band gap. The extrapolation of $h\nu$ at $\varepsilon = 0$ gives absorption edge energy corresponding to E_g = 2.67 eV for 2 : 1 Co/Ti LDH, which is found to be much smaller than that of pure NiO (~2.94 eV), ZnO (~3.23 eV), ZnS (~3.54 eV), CoO (~2.68 eV), TiO2 (~3.25 eV) and Degussa P25 (~3.18 eV).

The narrow band gap imparts better semiconducting properties to Co/Ti LDH in comparison to the commercial ZnO, ZnS, CoO, TiO_2, NiO and Degussa P25. Moreover, a red shift is observed in the UV-visible spectrum of the LDH, which could be attributed to the narrow band gap, suggesting that photo-generated e^--h^+ pairs could be generated by the LDH through irradiation with longer wavelength of visible light.[30] The presence of narrow band gap in the LDH could be attributed to localized gap states induced by Ti^{3+} accompanied by oxygen vacancies within the layered framework. This is also confirmed by PL and XPS

observations. The narrow band gap imparts excellent photocatalytic properties to the LDH for degradation of dye-stuffs than that of other commercial photocatalysts.

3.9. Thermogravimetric analysis

The TG measurements showed three degradation steps for Co/Ti LDH (Fig. S4; ESI†), which indicated that the thermal stability of the synthesized LDH was very much comparable with that of other LDHs.[3,8] Weight loss between 83–130 °C with a peak at ~89 °C, indicated by the DTG curve, could be assigned to the loss of physisorbed and interlayer water constituting ~13% by weight of the material. The second loss, observed from ~240 to 293 °C with a sharp peak at 262 °C, accounted for 17% weight loss, and was obviously due to dehydroxylation of the brucite like layers. The third weight loss of ~22% from 294 to 430 °C, associated with a broad peak at 335 °C, is likely to have occurred due to the decomposition of the interlayer CO_3^{2-} ions.[17,18]. No further weight loss was observed above 450 °C, which indicated the presence of very negligible amount of carbonaceous residues in the LDH. The thermogravimetric data have been found to be in agreement with XRD and FT-IR results, indicating the presence of H_2O and CO_3^{2-} ions in the interlayer galleries of the layered nanomaterial.

3.10. Morphology and particle size distribution

The morphology of 2 : 1 Co/Ti LDH was investigated using HRTEM, SEM and AFM measurements. The HR-TEM micrograph [Fig. 10(A)] shows ultra-fine hexagonal shaped particles with stacking of one layer over the other, in good agreement with the SEM results [Fig. 10(E)]. The bright spots in the SAED pattern reveal crystalline nature of the LDH [Fig. 10(B)] with a well ordered house-of cards type stacking. The interlayer distance of the periodic lattice fringes of (003) plane of 2 : 1 Co/Ti-LDH could be measured as ~0.763 nm from HR-TEM analysis [Fig. 10(C)], which is in accordance with that obtained from X-ray diffraction studies of Co/Ti LDH (Table S2, ESI†). The average particle size was calculated to be around 104 nm; evident from the histogram plot [Fig. 10(D)]. The cross-sectional TEM analysis (Fig. S5; ESI†) yielded the distance between two consecutive brucite sheets to be 0.39 nm and the thickness of the brucite like metal hydroxide layer to be 0.42 nm. The sum of the interline distances (brucite like sheet thickness + interlayer thickness) is 0.81 nm, which is in good agreement with the C' lattice parameter of the LDH determined from XRD data (Table S2, ESI†).

The SEM micrograph [Fig. 10(E)] showed regular hexagonal platelets, consistent with the TEM results. The presence of a large number of platelets could be an evidence of subsequent crystallization of layered double hydroxide incorporated with CO_3^{2-} and H_2O molecules in the interlayer.[19–24] The presence of CO_3^{2-} in the interlayer galleries of the LDH has produced a change in the superficial interaction between the particles influencing the stacking pattern and resulting in the formation of a 3D architecture accompanied by pores of different sizes, as determined from the surface area measurements.

The tapping mode AFM micrograph [Fig. 10(G)] also confirms the presence of hexagonal platelets, thereby supporting the HR-TEM and SEM results. The LDH particles possess regular hexagonal shapes with 120° internal angles, reminiscent of the hexagonal

morphology of the Co/Ti LDH. The parallel layer-by-layer house-of-cards packing of brucite like layers was further confirmed by AFM observations. The formation of flat crystallite terrace in the height profile of crystallites [Fig. 10(H and J)], provides strong evidence for a parallel multilayered structure, which is also consistent with the cross-sectional TEM results. Fig. 10(I) represents the 3D AFM micro-graph where the darker zones (between the hexagonal plates) represent the voids in the hexagonal LDH platelets. The number of parallel LDH layers could be calculated though the total thickness along c-axis and was found to be ~31 nm from the height profile AFM of LDH crystallites. Dividing the total thickness of Co/Ti LDH with the lattice parameter C' obtained from XRD results, it is confirmed that Co/Ti LDH comprises of 38 to 39 parallel house-of cards type brucite like layers.

The elemental composition of 2 : 1 Co/Ti LDH was investigated using energy-dispersive X-ray spectroscopy (EDX) [Fig. 10(F)]. The EDX analysis indicates the presence of Co, Ti, O, Cl, C and N in the LDH having Co/Ti atomic ratio of 2.03 : 1, in good agreement with the Co/Ti nominal ratio (2 : 1) taken for the synthesis. The EDX data are listed in Table 1. The fractionally higher atomic ratio of Co/Ti in the synthesized LDH, might have resulted due to the presence of CoO_x impurity in the hydrated cobalt nitrate salt used as a precursor of Co during LDH synthesis.

3.11. Photocatalytic reactions

The catalytic activity of the semiconductor Co/Ti LDH depends on the surface area, narrow band gap, light harvesting capacity and separation of e^--h+ pairs by absorption of incident photons with energies larger than its band gap energy (E_g). The ability of e^--h^+ pair separation in 2 : 1 Co/Ti LDH is evident from the luminescence spectra and EIS analyses. The high specific surface area, narrow band gap and presence of different surface states accompanied by oxygen vacancies, as evident from BET, DRS and XPS analyses, indicate the potential of the LDH to generate e^--h^+ pairs easily under visible light, resulting in its highly efficient photocatalytic activity.

The photocatalytic reactions of 2 : 1 Co/Ti LDH were carried out with aqueous Congo Red (CR), with the LDH dispersed in 200 ml aqueous solution of the test dye, followed by vigorous stirring of the reaction mixture for 30 min in the dark for establishing adsorption equilibrium between the LDH and the dye (S7, ESI†). This was followed by irradiation of the experimental mixture with visible light. It has been observed that the synthesized LDH exhibited better photocatalytic degradation of CR (at pH = 4) than commercial ZnO, ZnS, CoO, TiO_2, NiO and Degussa P25. The photocatalytic experiments were done with variation of pH, catalyst amount, variation of molar ratios of Co/Ti in the LDH and initial dye concentration. The photocatalytic effects were also studied separately with respect to influence of different quenchers like 2Na-EDTA (h^+ scavenger), *n*-butanol ($^\bullet OH$ scavenger), benzoquinone ($O_2^{\bullet-}$ scavenger) by adding the same at the beginning of the dye degradation experiment in order to indirectly establish the role played by $^\bullet OH$, h^+ and $O_2^{\bullet-}$ species in the photodegradation process. The reaction was monitored by following the decrease in the absorption intensity of the dye at λ_{max} = 497 nm in 15 min intervals with a Shimadzu 1800 UV-vis spectrophotometer. The extent of decolorization was obtained from the ratio C/C_0,

where C and C_0 were the absorbance values at a particular time interval and at $t = 0$ respectively. The strong absorption bands of CR decreased gradually on increasing irradiation time and the absorbance of the dye decreased nearly to zero after 75 min of visible light irradiation with the synthesized LDH [Fig. 11(A)]. The solution colour changed to nearly transparent marking the end of the decolorization [Fig. 11(B)]. The highly efficient photocatalytic performance of the synthesized Co/Ti-LDH compared to ZnO, ZnS, TiO_2, CoO, NiO and Degussa P25 could be attributed to the presence of high surface area, defects, oxygen vacancies and Ti^{3+} centers within the layered brucite like structure.[8,15,23] Control experiments like blank and dark reactions revealed negligible adsorption, clearly indicating that visible light plays a significant role in the photodegradation process.

3.11.1. Effects of catalyst amount.—In photocatalytic processes, catalyst amount is an important factor that controls the rate of degradation and hence, it is extensively studied. The photocatalytic experiments were carried out using Co/Ti LDH of different loadings (5.0 to 20.0 mg in 200 ml CR solution) with a fixed dye concentration (1×10^{-5} M) and irradiation time of 75 min. Fig. 12(A) displays the percentage decolorization of CR. The optimum efficiency is obtained with LDH dose of 15.0 mg than the others. Heterogeneous photocatalytic reactions are known to show proportional increase in photodegradation with catalyst loadings.[2,8] Generally, in any given photocatalytic application, the optimum catalyst concentration must be determined, in order to avoid excess catalyst and ensure total absorption of efficient photons. This is due to unfavourable light scattering and reduction of light penetration into the solution with excess photocatalyst loading. Thus, a decrease in degradation efficiency was observed when the LDH dose was further increased to 20.0 mg. On the basis of the observations, the catalyst loading was kept at 15.0 mg in the degradation experiments for maximum performance.

3.11.2. Effects of pH.—The pH is a very important parameter which controls the extent of photoassisted degradation. The effects of pH on degradation of CR were investigated using 15.0 mg of LDH; 1×10^{-5} M CR solution in the pH range of 4.0 to 11.0, adjusted by addition of either 0.1 M HCl or NaOH. The plot of C/C_0 *vs.* irradiation time of aqueous CR is presented in Fig. 12(B). The efficiency of photodegradation of aqueous CR was found to be higher in the acidic medium particularly at pH 4 (~99.7%) because Co/Ti LDH surface was highly positive at this pH, indicated by the zeta potential results, creating strong electrostatic interaction with the negatively charged CR ions. At pH > pH_{zpc}, the LDH surface is negatively charged, repelling the dye anions from the catalyst surface and correspondingly, CR degradation declines.[8]

3.11.3. Effects of initial dye concentration.—The effects of dye concentration are very important from the application point of view. Maximum efficiency was observed at pH 4 with 15.0 mg of Co/Ti LDH [Fig. 13(A)]. At the dye concentration of 1×10^{-5} M, 99.7% degradation could be achieved with aqueous CR at room temperature (~30 °C). The degradation decreased to 80% and 71% for aqueous CR of 1×10^{-4} M and 1×10^{-3} M concentrations respectively.

The reason for the observed changes could be linked to more and more dye molecules getting adsorbed on the LDH surface when the initial dye concentration was increased. The

large amount of adsorbed dye molecules could have caused an inhibitive effect on the photocatalytic degradation due to the lack of direct contact among the photogenerated holes, hydroxyl radicals or superoxide radicals. Moreover, high dye concentration may act as inner filter which shunts the photons away from the LDH surface. Most of the dye molecules after getting adsorbed on the LDH surface might also block the active surface sites for reaction decreasing the photo-degradation efficiency.[8]

3.11.4. Effects of variation of Co/Ti ratio.—In order to achieve optimum photocatalytic performance, 1 : 1, 3 : 1 and 4 : 1 Co/Ti LDHs were also synthesized (S8; ESI†) and were used for comparing the photodegradation performances with that of 2 : 1 Co/Ti LDH. The comparative photodegradation analysis was done at pH 4 with 15.0 mg of LDH and 1×10^{-5} M CR solution. Fig. 13(B) shows that 2 : 1 Co/Ti LDH exhibited much higher activity than that of either of the other Co/Ti LDHs. These results suggest a synergistic effect between Co and Ti in the LDH for exhibiting maximum photocatalytic performance. It is most likely that 2 : 1 Co/Ti LDH provides an optimum contact surface for Ti-species and the visible light photons, giving maximum photocatalytic performance.[31]

3.11.5. Recyclability of 2 : 1 Co/Ti LDH.—After each degradation cycle, the LDH was separated from the reaction system, was regenerated by washing it three times with de-ionized water followed by drying, and was reused as a photocatalyst. The degree of CR degradation for the first cycle was ~99.7% [Fig. 13(C)]. Although the extent of degradation of the LDH declined in the second, third, fourth and fifth cycles, the rate of photodegradation was still 92% after the fifth cycle indicating that the synthesized LDH is a potential recyclable candidate for photodegradation purposes.

3.11.6. FT-IR analysis of Co/Ti-LDH before and after degradation.—In order to evaluate the photostability of 2 : 1 Co/Ti LDH after the fifth cycle of CR degradation, the FT-IR analysis of the LDH and that recovered at the end of the fifth cycle of CR degradation was carried out (Fig. 14). The comparative analysis reveals that the LDH showed remarkable photostability even after fifth cycle of use with all the characteristic IR-bands present in their respective positions, accompanied by some minor changes in the fingerprint region.[32–34]

3.11.7. Effect of quenchers on photodegradation.—The photodegradation reactions catalyzed by the LDHs are driven mainly by quenchers like ·OH, h+ and O·⁻. In order to evaluate their respective roles in the photocatalytic activity of CR, the quenchers were added externally to the reaction mixture at the beginning of the degradation experiments to elucidate the semiconduction mechanism of photocatalysis.30–33 The photo-catalytic effects of the ·OH, h+ and O2·− species, are illustrated in Fig. 15(A). It is observed that the degradation of aqueous CR was suppressed on addition of quenchers like n-butanol, (scavenger of ‘OH), disodium ethylenediaminetetraacetate (h^+ scavenger) and benzoquinone (BQ) ($O2^-$ scavenger), indicating that ·OH, h+ and $O2^-$ radicals were the main active species generated on the LDH surface under visible light, which contribute to the degradation of CR. These results are in accordance with the XPS, EIS and PL observations, signifying that the photocatalytic reactions of Co/Ti LDH are governed mainly by these species.[8,13]

3.11.8. Kinetics of CR degradation.—The photodegradation kinetics of aqueous CR dye was investigated at pH 4 under optimum conditions (catalyst 15.0 mg; dye concentration 1×10^{-5} M) in order to understand the reaction characteristics of the anionic CR dye under visible light catalysed by 2 : 1 Co/Ti LDH. The observed linearity in the plot of $\ln(C_0/C)$ vs. irradiation time [Fig. 15(B)] signifies that the degradation of the test dye follows pseudofirst-order kinetics, represented by the equation

$$\ln\left(\frac{C_0}{C}\right) = k_{app}t \quad (4)$$

where C_0 is the initial concentration of the dye and C is the concentration at time t. The apparent rate constant kapp was found to be 0.043 min^{-1}. The half life was found to be 16.12 min, calculated from k_{app} by using the relation:

$$t_{1/2} = \frac{\ln 2}{k_{app}} \quad (5)$$

Thus, the photodegradation of CR is primarily dependent on the light intensity and absorption efficiency of the Co/Ti LDH.[2,8,16]

3.11.9. Comparative degradation of 2 : 1 Co/Ti LDH w commercial catalysts.—A comparative photodegradation analysis was performed to validate the efficiency of Co/Ti LDH over commercial ZnO, ZnS, CoO, TiO_2, NiO and Degussa P25 for degradation of the anionic CR dye. As maximum efficiency of Co/Ti LDH was observed at pH 4 with 15.0 mg LDH in 200 ml dye solution of concentration 1×10^{-5} M at room temperature (30 °C), the comparative studies were done under these conditions with all the catalysts. 2 : 1 Co/Ti-LDH showed enhanced degradation of the dye (~99.7%) in 75 min in comparison to ZnO (~66%), CoO (~82%), TiO_2 (~49%), ZnS (~59%), NiO (~83%) and Degussa P25 (~76%) as observed from C/C_0 vs. irradiation time plots [Fig. 16(A)]. Thus, the dye solution became colourless in 75 min with Co/Ti LDH indicating a higher efficiency for CR degradation than the other commercial catalysts.8 Blank reaction (without the catalyst) under the same experimental conditions showed ~18% adsorption, attributed to the effects of the visible light on adsorption of the anionic dye while the dark showed ~25% adsorption of CR from aqueous solution.

3.11.10. FT-IR analysis of the end products of photodegradation.—In order to investigate the existence of adsorption or degradation in the decolorization of CR, a comparative FT-IR analysis of the end products (after centrifugation of the mixture from the dark, blank and photocatalytic reactions with 2 : 1 Co/Ti LDH) was undertaken along with that of pure CR [Fig. 16(B)]. It is seen that all the characteristic bands were present at their respective positions for both blank and dark reactions with some peaks becoming broad particularly in the fingerprint region, clearly indicating the occurrence of adsorption in the control experiments. However, the FT-IR spectrum of aqueous CR solution after 75 min (at

the end of the decolorization process) indicates the absence of most of the characteristic bands of the anionic dye with some band shifts being observed to newer positions, indicating that 2 : 1 Co/Ti LDH has remarkable ability to degrade the anionic CR dye to simple molecules under visible light irradiation.

3.11.11. Semiconduction pathway of photoassisted degradation.—Depending on electrochemical impedance, XPS, DRS, PL and indirect radical and hole trapping experiments, a semiconduction mechanistic pathway for photodegradation of aqueous CR with 2 : 1 Co/Ti LDH is proposed on the basis of band theory by taking O1s orbital as the valence band, Co2p and Ti2p orbitals as the conduction bands. The photocatalytic degradation is supposed to take place in two different pathways by the generation of reactive species like OH and $O2^-$ in presence of visible light.

First pathway.: It is proposed that the series of reactions take place in the following sequential pattern (eqn (6)–(17)) upon visible light exposure at 30 °C. The electrons are first excited from valence band to the conduction band, thereby leaving holes in the valence band. The absorption of photons initiates electronic excitation with energy equal to or greater than the band gap energy of the semiconductor, Co/Ti LDH. Thus, 2 : 1 Co/Ti-LDH generates e^--h^+ pairs (eqn (6)) upon visible light exposure, thereby reducing Co^{3+} and Ti^{4+} species on the LDH surface (eqn (7)–(9)). This generates a strong redox reaction (eqn (9)) being initiated by the photo-generated electrons with intense lattice vibrations on the LDH surface. The hopping h^+ move to the LDH surface and react with H_2O and OH^- ions yielding OH radicals (eqn (10) and (11)). The e^- are likely to react with adsorbed oxygen present on the surface to produce superoxide ($O2^-$) (eqn (12)). Superoxide ($O2^-$) further reacts with adsorbed H^+ present on the surface to produce peroxide radicals (OOH) (eqn (13)), further yielding H_2O_2 (eqn (14)) and hydroxyl radicals (OH) (eqn (15)). Hydroxyl (OH) and superoxide ($O2^-$) radicals are highly active species that mineralize the dye to simple molecules (eqn (16)). The photo-generated, h^+ and e^-, may also recombine and dissipate the energy as light or heat (eqn (17)) which reduces the quantum efficiency.[8] The first pathway proceeds through the following set of sequential reactions

$$\text{Co/Ti LDH} + h\nu \rightarrow \text{Co/Ti LDH}\left(e^- + h^+\right) \quad (6)$$

$$Co^{3+} + e^- \rightarrow Co^{2+}(\text{electron trap}) \quad (7)$$

$$Ti^{4+} + e^- \rightarrow Ti^{3+}(\text{electron trap}) \quad (8)$$

$$Co^{3+} + Ti^{4+} + h\nu \leftrightarrow Co^{2+} + Ti^{3+}(\text{migration}) \quad (9)$$

$$h^+ + H_2O \rightarrow {}^{\cdot}OH + H^+ \quad (10)$$

$$h^+ + OH^- \rightarrow {}^{\cdot}OH \quad (11)$$

$$O_2 + e^- \rightarrow O_2^{\cdot -} \quad (12)$$

$$O_2^{\cdot -} + H^+ \rightarrow HOO^{\cdot} \quad (13)$$

$$HOO^{\cdot} + HOO^{\cdot} \rightarrow H_2O_2 + O_2 \quad (14)$$

$$H_2O_2 + O_2^{\cdot -} \rightarrow {}^{\cdot}OH + OH^- + O_2 \quad (15)$$

$$\text{CR dye} + O_2^{\cdot -} + {}^{\cdot}OH \rightarrow \text{degradation products} \quad (16)$$

$$h^+ + e^- \rightarrow \text{energy} \quad (17)$$

Second pathway.: The second pathway proceeds through the photosensitization of the CR dye in the presence of visible light.[35–37] In this process, the dye molecules act as sensitizer by absorption of visible light to yield an excited state of the sensitizer (eqn (18)), which further transforms to dye radicals with the release of electrons (eqn (19)). The dye radicals thus generated form intermediate products like CO_2 and H_2O (eqn (20)). The electrons are injected into the conduction band of the Co/Ti LDH photocatalyst (eqn (21)) where they are scavenged by O_2 to form $O2^-$ species as shown (eqn (22)), yielding H_2O_2 (eqn (23)). The electron transfer from the excited dye molecule to the conduction band of LDH is very fast (in the range of tens of femtoseconds). H_2O_2 subsequently generates OH radicals (eqn (24)) that degrade the complex dye to simple molecules (eqn (25)).

$$\text{Dye} + h\nu \rightarrow \text{dye}^* \quad (18)$$

$$\text{Dye}^* \rightarrow \text{dye}^{\cdot +} + e^- \quad (19)$$

$$\text{Dye}^{\cdot +} \rightarrow CO_2 + H_2O \quad (20)$$

$$\text{Co/Ti LDH} + e^- \rightarrow \text{Co/Ti LDH}^{\cdot +} \quad (21)$$

$$\text{Co/Ti LDH}^{\cdot +} + O_2 \rightarrow \text{Co/Ti LDH} + O_2^{\cdot -} \quad (22)$$

$$O_2^{\cdot -} + 2H_2O + e^- \rightarrow 2H_2O_2 \quad (23)$$

$$H_2O_2 + e^- \rightarrow {}^{\cdot}OH + OH^- \quad (24)$$

$${}^{\cdot}OH + \text{CR dye} \rightarrow \text{degradation products} \quad (25)$$

These observations clearly demonstrate the involvement of holes (h^+), hydroxyl (OH) and superoxide ($O2^-$) species as highly reactive agents in the Co/Ti LDH mediated photocatalytic degradation of the anionic Congo Red in aqueous medium. The XPS and the PL measurements suggest that both Co and Ti are present in two oxidation states, accompanied by oxygen vacancies in the LDH. The presence of defects and O_2/O_2^- transformation in the LDH has also been confirmed by EIS and PL analyses. DRS also indicate the presence of Ti^{4+} in brucite sheets. The broad nature of absorption at ~548 nm could be ascribed to supramolecular guest-guest or guest-host interactions. On the basis of these data, the mechanistic pathways has been presented in the form of e^--h^+ hopping conduction model and through photosensitization of the dye. The schematic illustrations of the mechanistic pathways of photodegradation are represented in Fig. 17(A and B).

3.11.12. Analysis of end products of degradation and reaction mechanism.—

The decolorized end products of CR obtained after 75 min of visible light irradiation were further characterized by GC-MS to establish the reaction mechanism associated with CR degradation. The decolorized end products after centrifugation were extracted with dichloromethane and 1 μL of it was injected into the GC-MS analyser, the analysis was carried out in positive-ion mode. The mass spectrum is presented in Fig. 18.

The mass spectrum of the CR degradation products showed nine products. Congo Red is most likely to undergo asymmetric cleavage (Fig. 19) producing sodium(4-amino-3-diazenylnaphthalene)-1-sulfonate (2 molecules) and phenylbenzene (one molecule). Sodium(4-amino-3-diazenylnaphthalene)-1-sulfonate undergoes further dissociation forming sodium(4-amino-3-diazenyl-2-hydroxy)-1-naphthoxide (I) *(m/z* = 224), which transforms to form the compound (II) as well as 2-(1-amino-2-diazenyl-2-formylvinyl)benzoic acid (III) having *m/z* of 205 and 217 respectively. Sodium(4-amino-3-diazenylnaphthalene)-1-sulfonate is likely to undergo oxidation yielding 3-diazonium naphthalen-1-ol (IV) with a mass peak of 177, as intermediate product, which also undergoes transformation yielding 2-diazoniumnaphthalen-1,4-diol (V) with *m/z* of 192. Phenyl benzene is likely to undergo transformation to sodium phenyl phenoxide (VI) (*m/z* 196). It further reacts to form (VII) and (VIII) having *m/z* of 200 and 201 respectively, finally yielding 4-(4-oxocyclohexa-1,5-dienyl)cyclohex-4-ene-1,2-dione (IX) having m/z of 202. Apart from these peaks, the remaining region of the mass spectrum reveals some other peaks of negligible intensity, clearly indicating that most of the anionic CR dye molecules have been mineralized. The identification of the intermediates in the mass spectrum of Congo Red degradation products supports the asymmetric cleavage, leading to the formation of simple, less toxic molecules.

4. Conclusions

2 : 1 Co/Ti-LDH displayed remarkable photocatalytic properties for degradation of aqueous Congo Red. These properties of the LDH are attributed to the narrow band gap, high surface area, porous structure with surface defects and oxygen vacancies. The photocatalytic performance of the LDH is found to be much higher than that of commercial ZnO, ZnS, TiO_2, NiO and Degussa P25. It is observed that adsorption dominated the control experiments carried out in the dark as well as the blank reactions (without catalyst), whereas degradation marked the end of the photochemical reaction with the LDH. The catalytic activity of the LDH is retained even after the fifth cycle and the FT-IR analysis of the LDH before and at the end of the fifth cycle showed excellent photostability. The pseudo-first-order model satisfactorily describes the degradation kinetics. The strategy of applying urea solution as a basic precipitant as well as template in synthesizing Co/Ti LDH has been found to enhance its semiconducting catalytic properties. The mass spectrum analysis supported the asymmetric cleavage of the dye forming simple, less toxic and environment friendly molecules in show that 2 : 1 Co/Ti LDH could be potentially used as a very effective and recyclable photocatalyst for large scale wastewater treatment.

Supplementary Material

Refer to Web version on PubMed Central for supplementary material.

Acknowledgements

The authors sincerely thank Sanjeev K. Srivastava, Professor of Physics and Meteorology, IIT Kharagpur, India for helping with the XPS analysis of 2 : 1 Co/Ti LDH. The authors are also very grateful to the referees for suggesting certain important modifications to the manuscript.

References

1. Parida KM and Mohapatra L, Chem. Eng. J, 2012,179,131.
2. Silva CG, Bouizi Y, Fornes V and Garcia H, J. Am. Chem. Soc, 2009, 131, 13833. [PubMed: 19725513]
3. Chen D, Li Y, Zhang J, Zhou JZ, Guo Y and Liu H, Chem. Eng. J, 2012, 185–186, 120.
4. Xu S, Shen J, Chen S, Zhang M and Shen T, J. Photochem. Photobiol., A, 2002, 67, 64.
5. Zhang LW, Fu HB and Zhu YF, Adv. Funct. Mater, 2008, 18, 2180.
6. Chen G, Qian S, Tu X, Wei X, Zou J, Leng L and Luo S, Appl. Surf. Sci, 2014, 293, 345.
7. Xu ZP, Zhang J, Adebajo MO, Zhang H and Zhou C, Appl. Clay Sci, 2011, 53, 139.
8. Roy Chowdhury P and Bhattacharyya KG, Dalton Trans, 2015, 44, 6809. [PubMed: 25763803]
9. Zhang N, Yang MQ, Liu S, Sun Y and Xu YJ, Chem. Rev, 2015, 115, 10307. [PubMed: 26395240]
10. Zhao Y, Li B, Wang Q, Gao W, Wang CJ, Wei M, Evans DG, Duan X and O'Hare D, Chem. Sci, 2014, 5, 951.
11. Senthilnathan J and Philip L, Chem. Eng. J, 2010, 161, 83.
12. Comparelli R, Fanizza E, Curri ML, Cozzoli PD, Mascolo G and Agostiano A, Appl. Catal., B, 2005, 60, 1.
13. Zhang C, Gu L, Lin Y, Wang Y, Fu D and Gu Z, J. Photochem. Photobiol., A, 2009, 207, 66.
14. Zhao YF, Wei M, Lu J, Wang ZL and Duan X, ACS Nano, 2009, 3, 4009. [PubMed: 19928881]
15. Zhang J, Fu D, Gao H and Deng L, Appl. Surf. Sci, 2011, 258, 1294.
16. Huang Z, Wu P, Gong B, Fange Y and Zhu N, J. Mater. Chem *A*, 2014, 2, 5534.
17. Li K, Luo X, Lin X, Qi F and Wu P, J. Mol. Catal. A: Chem, 2014, 383–384, 1.
18. Ahmed AAA, Talib ZA and Hussein MZB, Appl. Clay Sci, 2012, 56, 68.
19. Tabet N, Faiz M and Al-Oteibi A, J. Electron Spectrosc. Relat. Phenom, 2008, 163, 15.
20. Baltrusaitis J, Jayaweera PM and Grassian VH, Phys. Chem. Chem. Phys, 2009, 11, 8295. [PubMed: 19756286]
21. Mehta SK, Kumar S, Chaudhary S and Bhasin KK, Nanoscale, 2010, 2, 145. [PubMed: 20648377]
22. Xu H and Zhang L, J. Phys. Chem. C, 2010, 114, 940.
23. Zou L, Xiang X, Wei M, Li F and Evans DG, Inorg. Chem, 2008, 47, 1361. [PubMed: 18193827]
24. Khan MM, Ansari SA, Pradhan D, Ansari MO, Hang DH, Lee J and Cho MH, J. Mater. Chem. A, 2014, 2, 637.
25. Galtayries A and Grimblot J, J. Electron Spectrosc. Relat. Phenom, 1999, 98–99, 267.
26. Bard AJ, Fan FRF, Gioda AS, Nagasubramanian G and White HS, Faraday Discuss. Chem. Soc, 1980, 70, 19.
27. Choudhury B, Dey M and Choudhury A, Appl. Nanosci, 2014, 4, 449.
28. Wang H, Xiang X, Li F, Evans DG and Duan X, Appl. Surf. Sci, 2009, 255, 6945.
29. Zou L, Xiang X, Fan J and Li F, Chem. Mater, 2007, 19, 6518.
30. Yang MQ, Zhang N, Pagliaro M and Xu YJ, Chem. Soc. Rev, 2014, 43, 8240. [PubMed: 25200332]
31. Zhang Y, Tang ZR, Fu X and Xu YJ, ACS Nano, 2010, 4, 7303. [PubMed: 21117654]
32. Li S, Bai Z and Zhao D, Appl. Surf. Sci, 2013, 284, 7.
33. Zhu Y, Zhou Y, Zhang T, He M, Wang Y, Yang X and Yang Y, Appl. Surf. Sci, 2012, 263, 132.
34. Cui GJ, Xu XY, Lin TJ, Evans DG and Li DQ, Ind. Eng. Chem. Res, 2010, 49, 448.
35. Yoshihara R, Katoh A, Furube Y, Tamaki M, Murai K, Hara S, Murata H, Arakawa M and Tachiya M, J. Phys. Chem. B, 2004, 108, 3817.
36. Liu S, Tang ZR, Sun Y, Colmenares JC and Xu YJ, Chem. Soc. Rev, 2015, 44, 5053. [PubMed: 25856797]
37. Zhang N, Zhang Y and Xu YJ, Nanoscale, 2012, 4, 5792. [PubMed: 22907128]

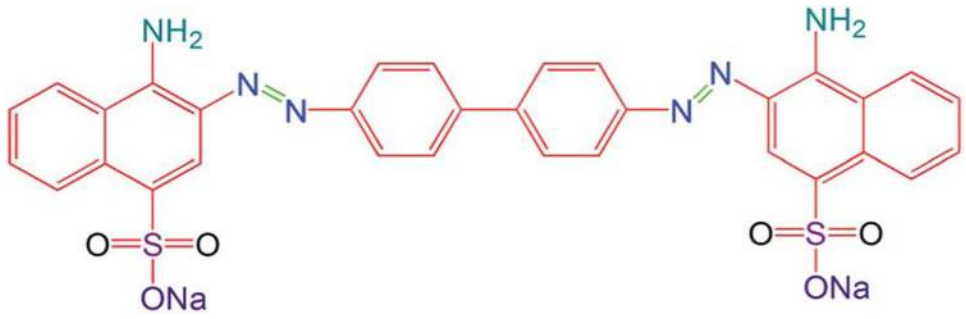

Fig. 1.
Structure of Congo Red.

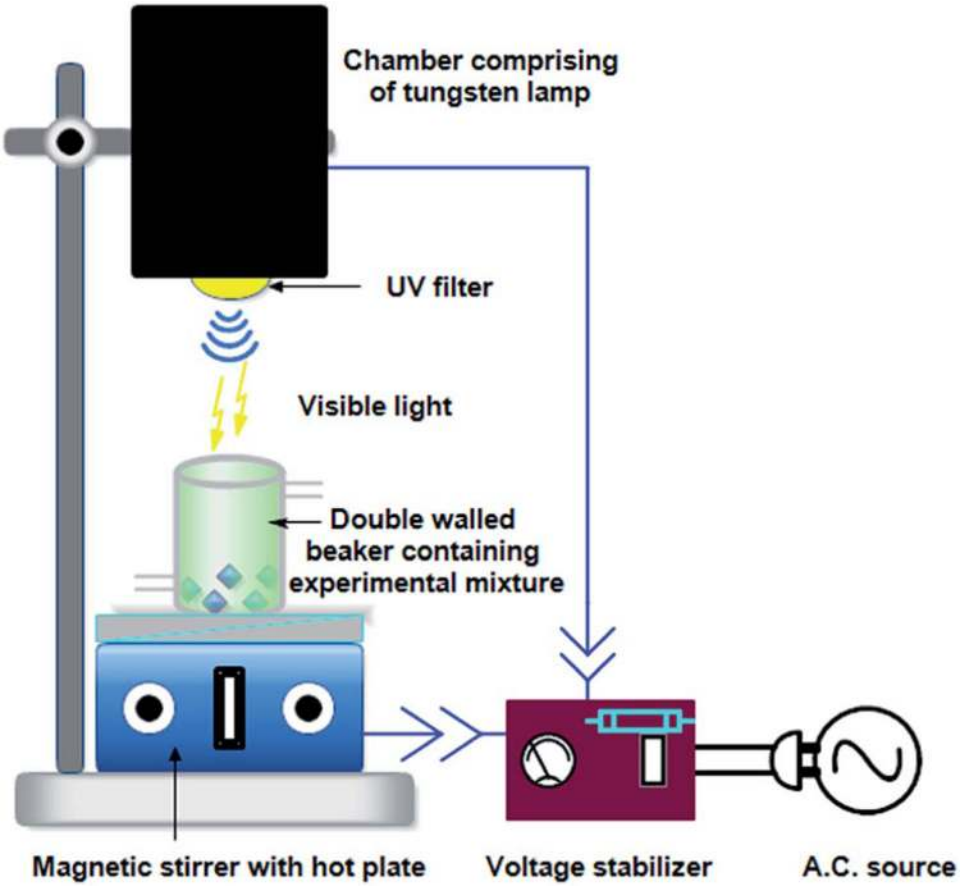

Fig. 2.
Schematic of the visible light photocatalytic set up.

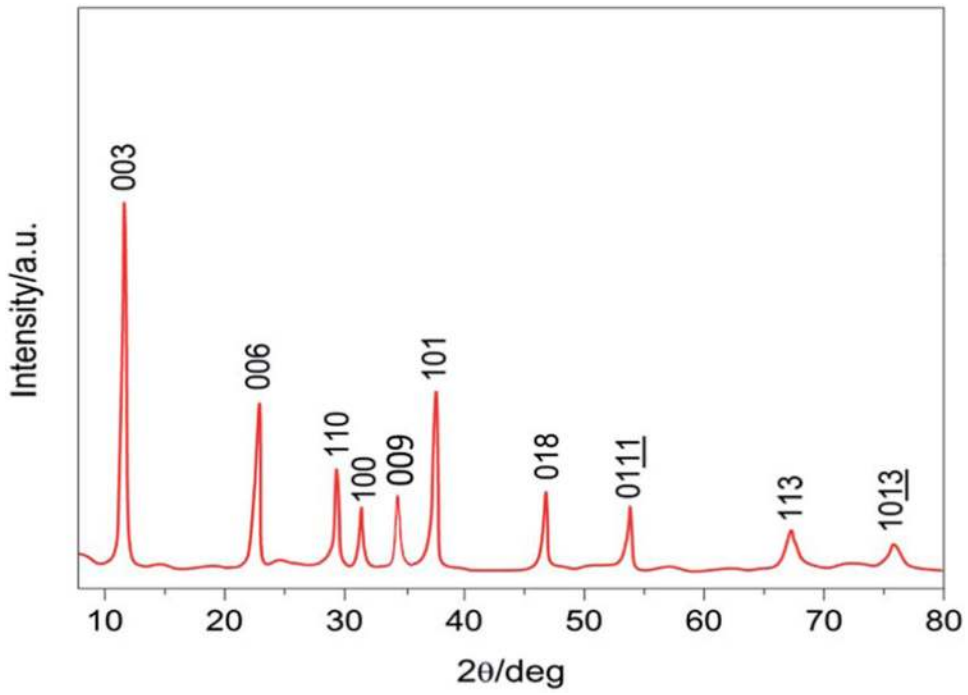

Fig. 3.
X-ray diffractogram of 2 : 1 Co/Ti LDH.

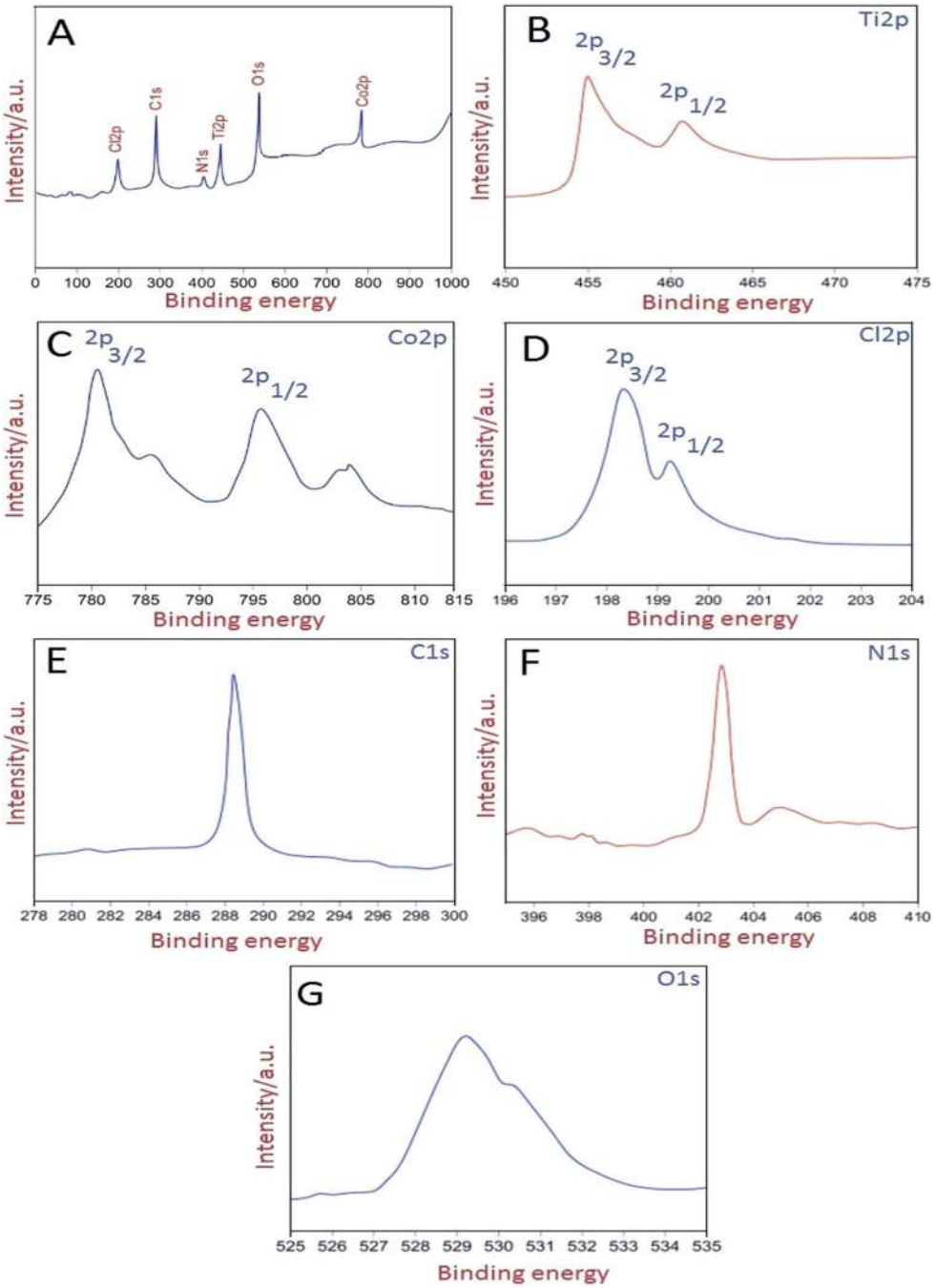

Fig. 4.

(A) XPS full surface survey (B) XPS Ti2p line (C) XPS Co2p line (D) XPS Cl2p line (E) XPS C1s line (F) XPS N1s line (G) XPS O1s line.

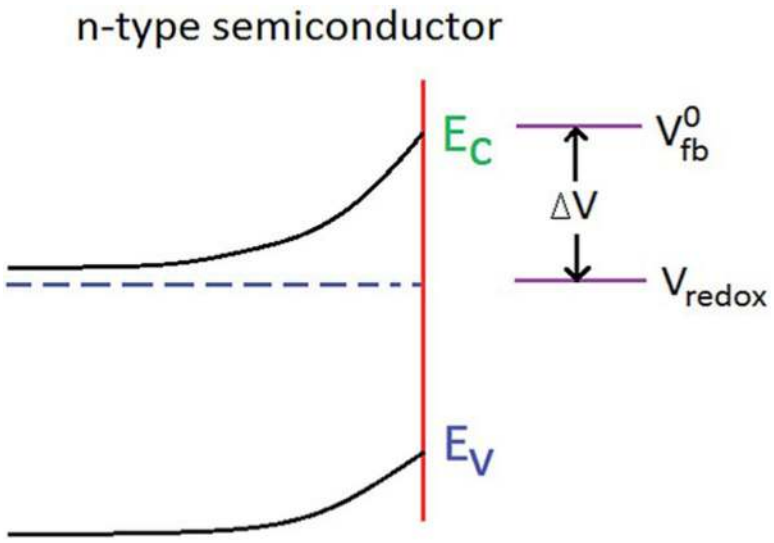

Fig. 5.
Scheme showing the model of surface state-free semiconductor.

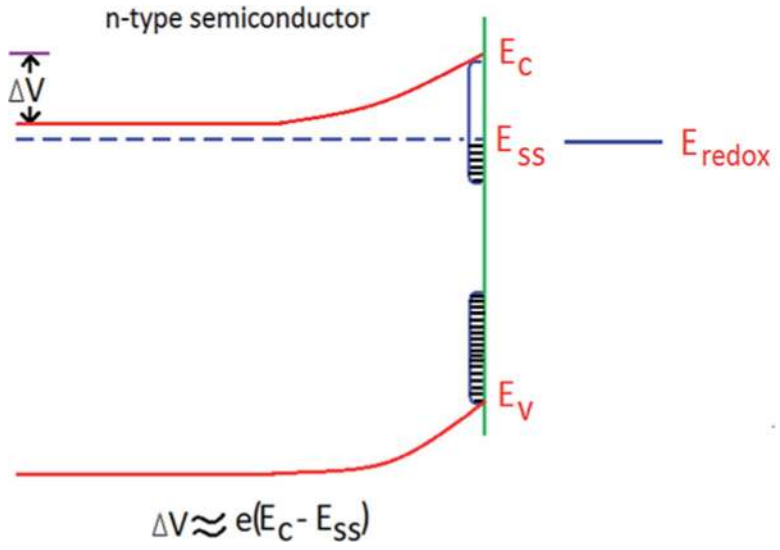

Fig. 6.
Scheme showing the Fermi level pinning of Co/Ti LDH (n-type semiconductor).

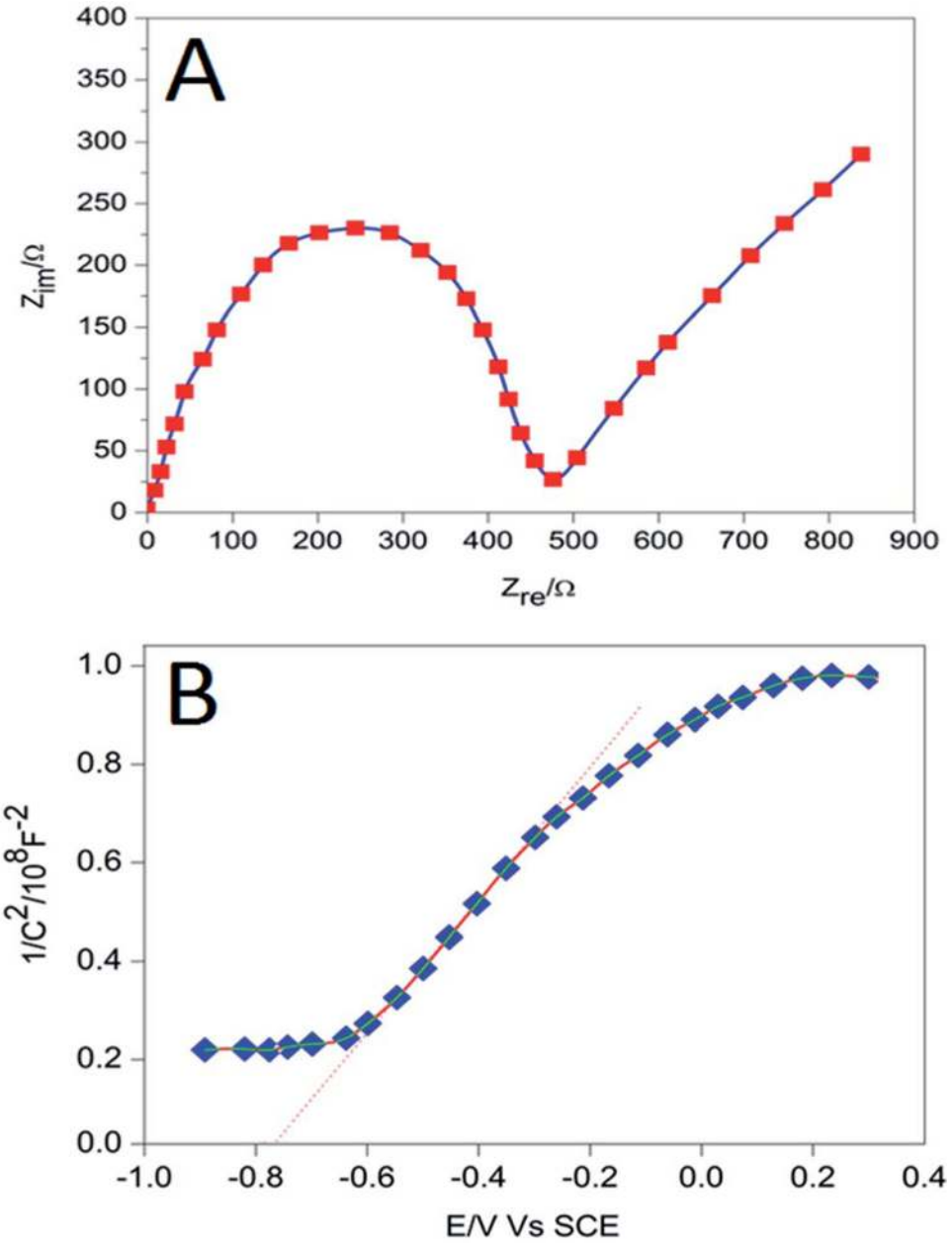

Fig. 7.

(A) Electrochemical impedance Nyquist plot and (B) Mott-Schottky plot of 2 : 1 Co/Ti LDH electrode.

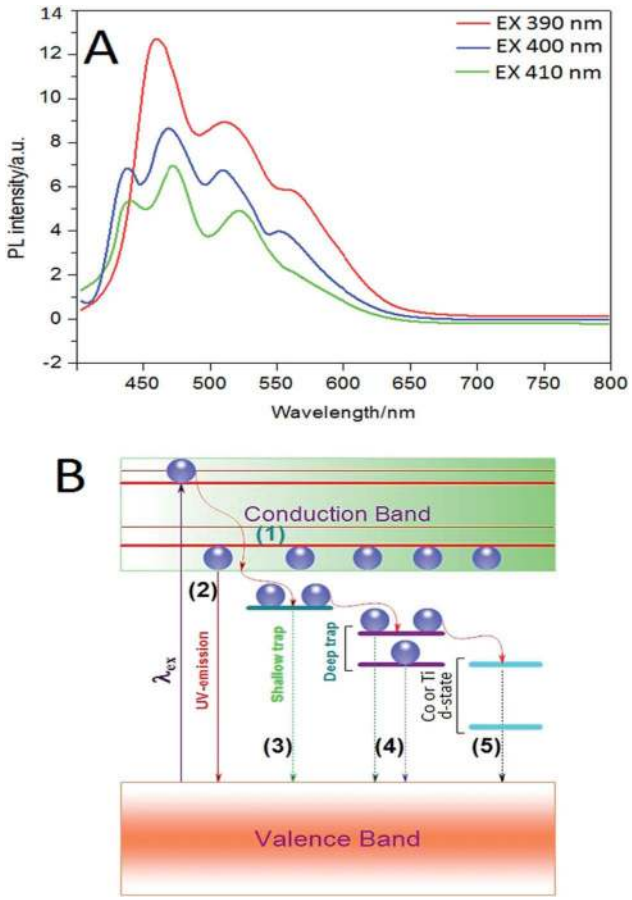

Fig. 8.

(A) Photoluminescence spectra at different excitation wavelengths (B) mechanism of photoluminescence emission of 2 : 1 Co/Ti LDH.

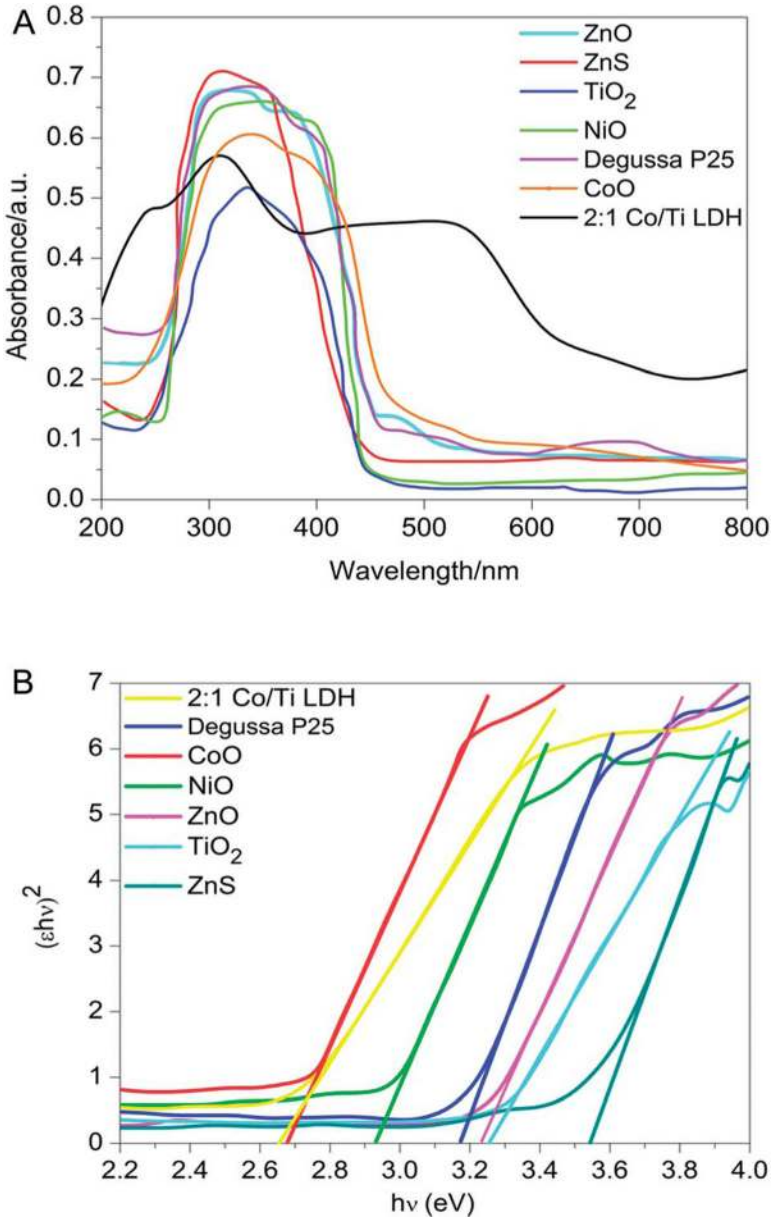

Fig. 9.

(A) UV-vis DRS of 2 : 1 Co/Ti LDH along with those of the commercial catalysts. (B) Tauc plot of 2 : 1 Co/Ti LDH with commercial catalysts.

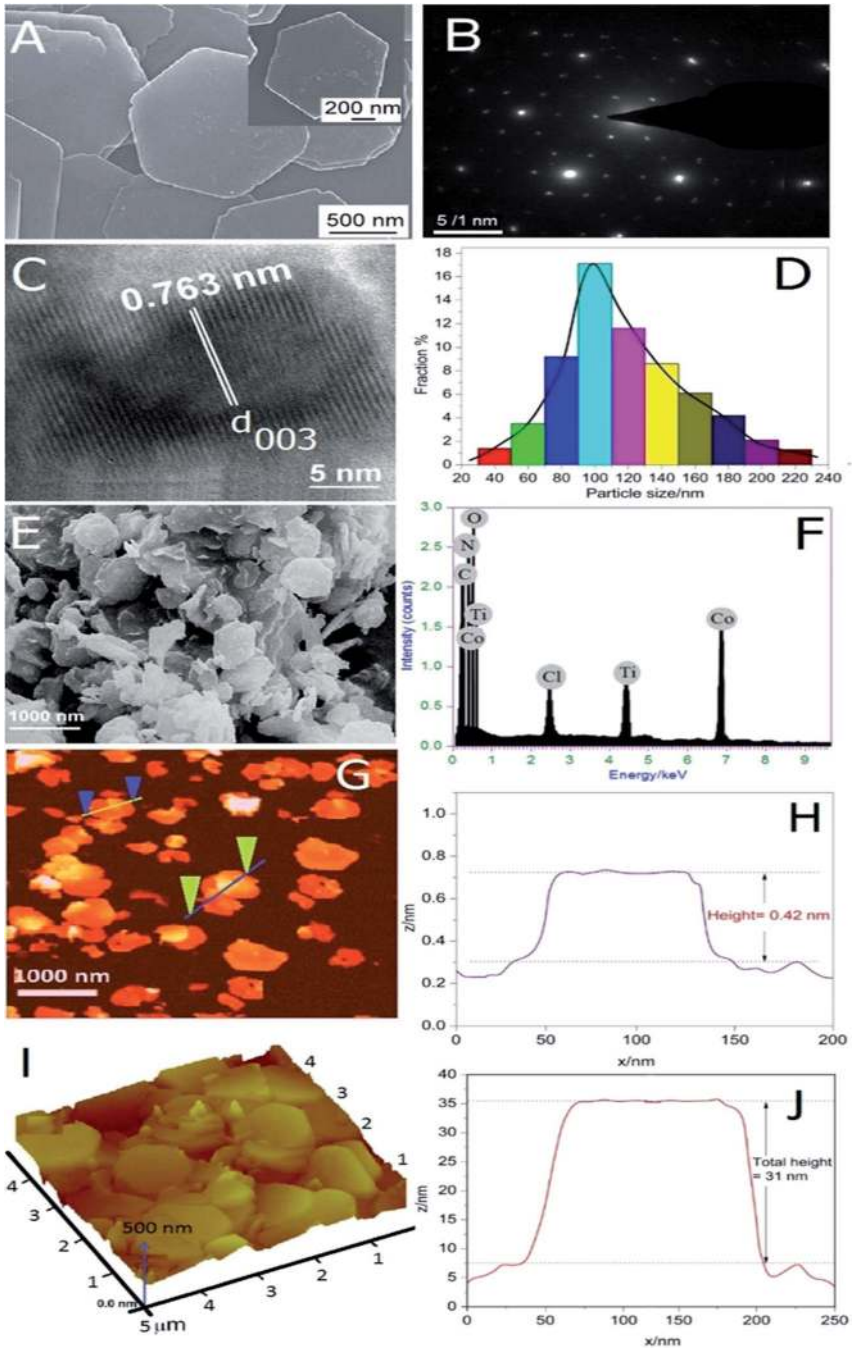

Fig. 10.

(A). HR-TEM image, (B) SAED pattern, (C) TEM image showing layered structure, (D) histogram plot, (E) SEM image, (F) EDX spectrum, (G) AFM micrograph, (H) height profile of single crystallite, (I) 3D AFM image, (J) total height profile of 2 : 1 Co/Ti LDH.

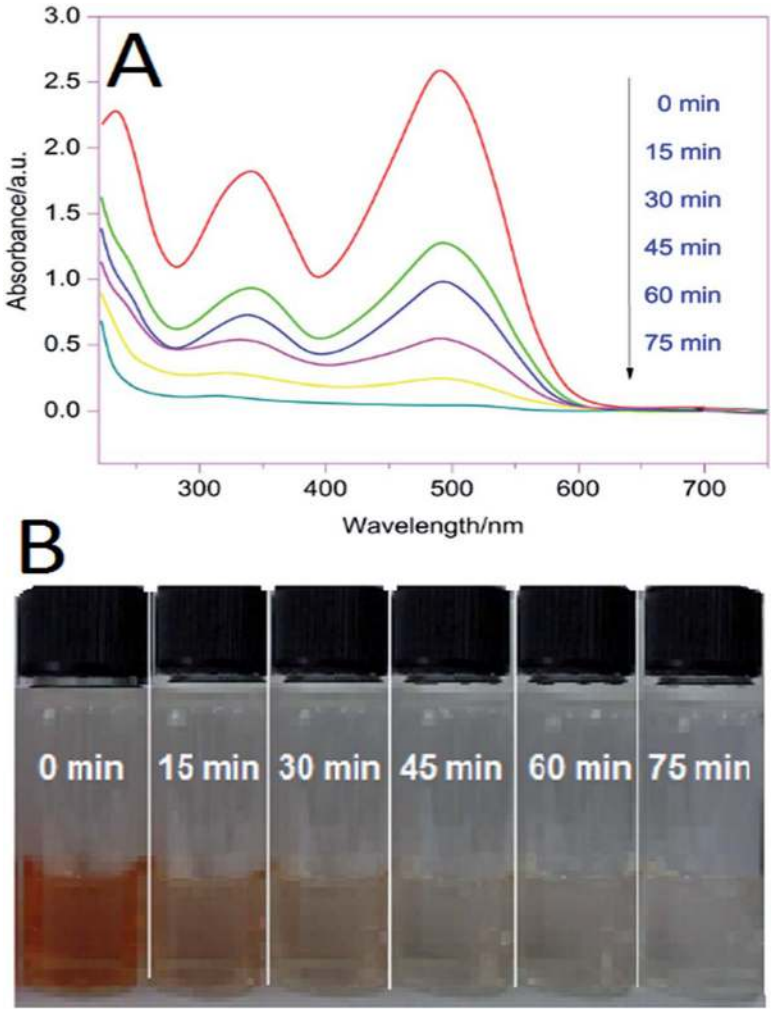

Fig. 11.

(A) UV absorption spectra of CR degradation with 2 : 1 Co/Ti LDH [pH 4.0; LDH 15.0 mg; aqueous Cr 1×10^{-5} M] (B) snapshot of aliquots of CR at different time intervals.

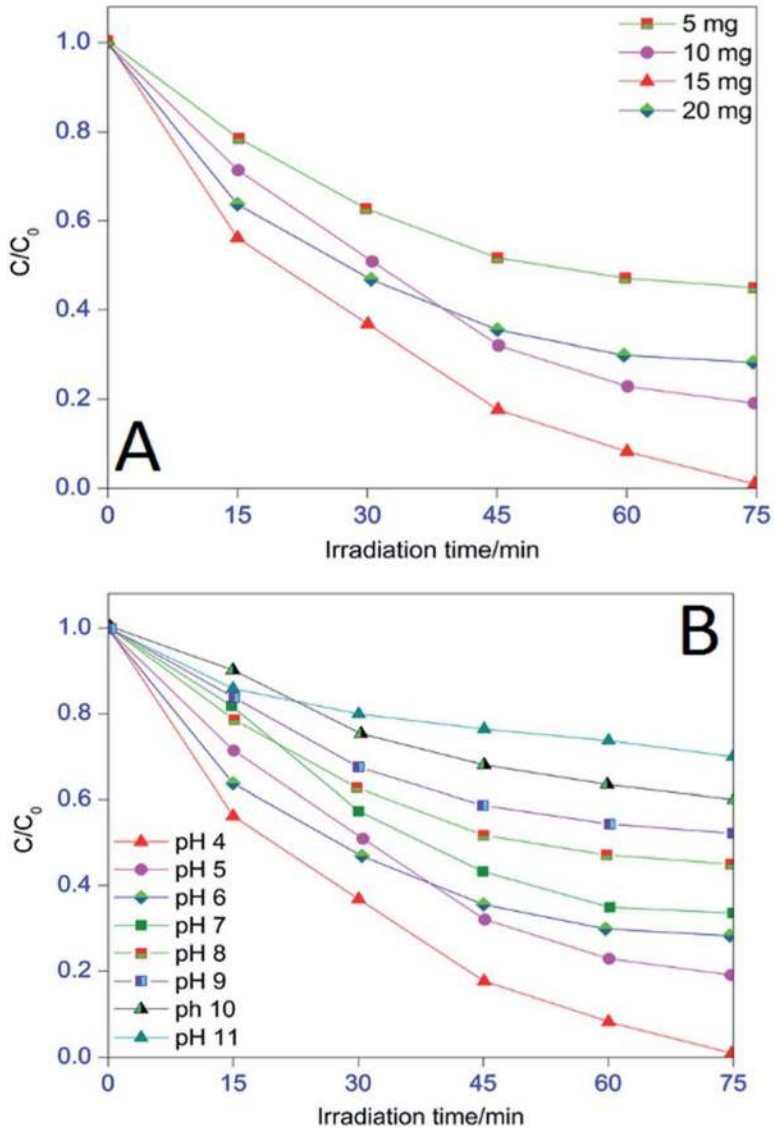

Fig. 12.

(A) Effects of catalyst amount and (B) effects of pH on photodegradation of aqueous Congo Red.

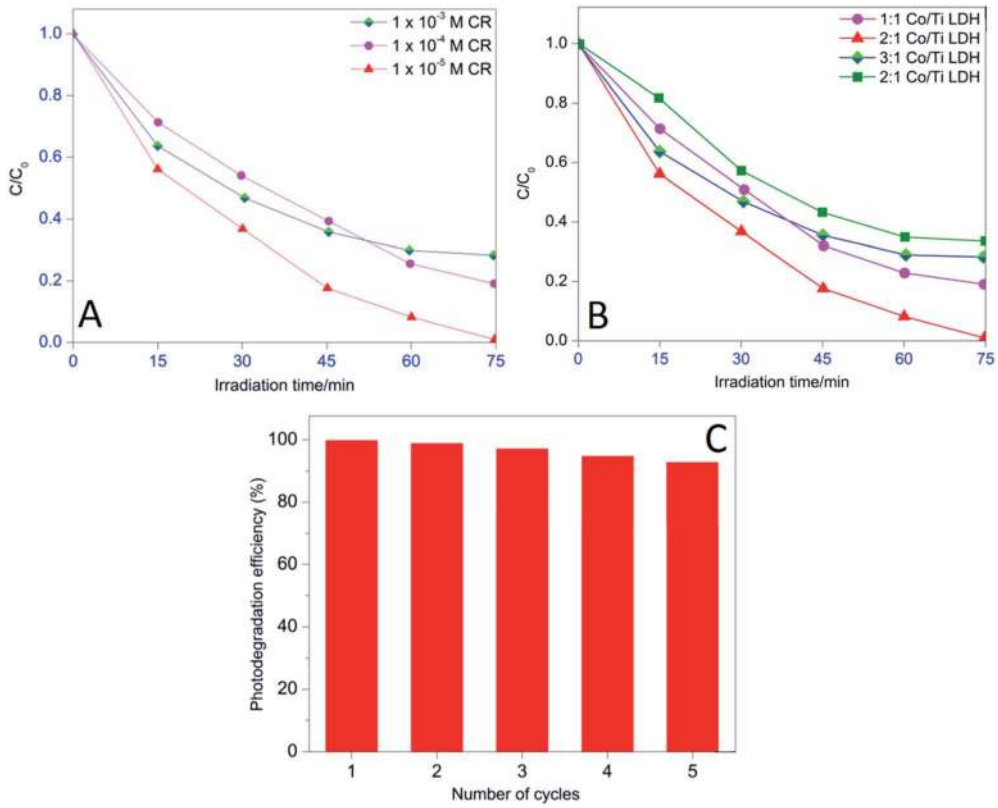

Fig. 13.

(A) Effects of initial CR concentration on degradation, (B) effects of variation of Co/Ti molar ratio in the LDH on degradation (C) number of recycles of 2 : 1 Co/Ti LDH.

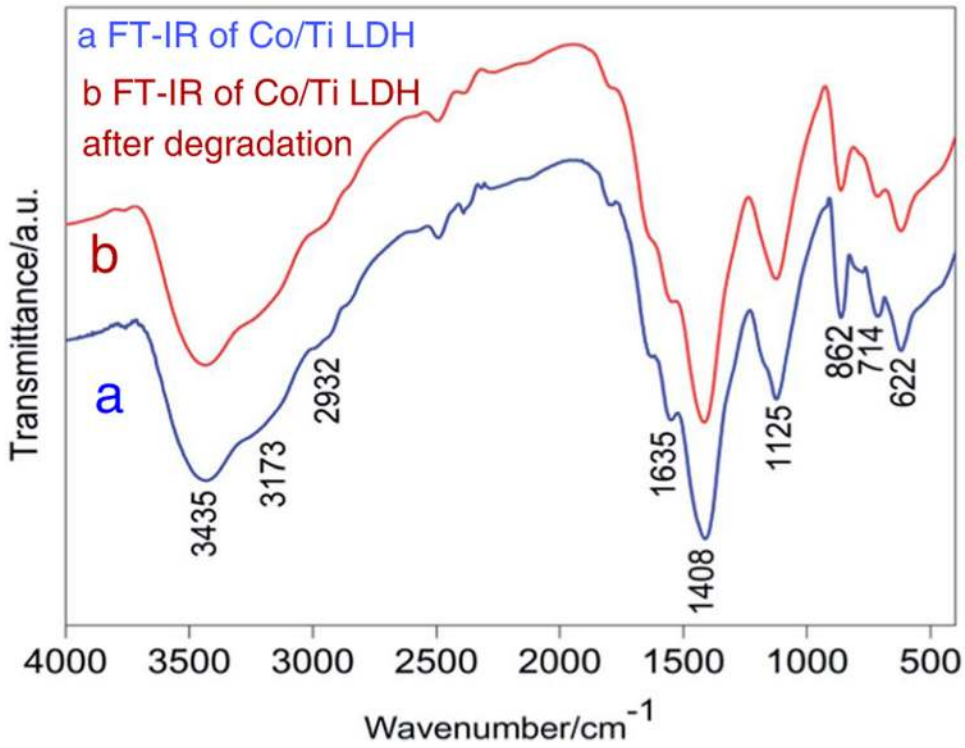

Fig. 14.
FT-IR analysis of Co/Ti LDH before and after degradation.

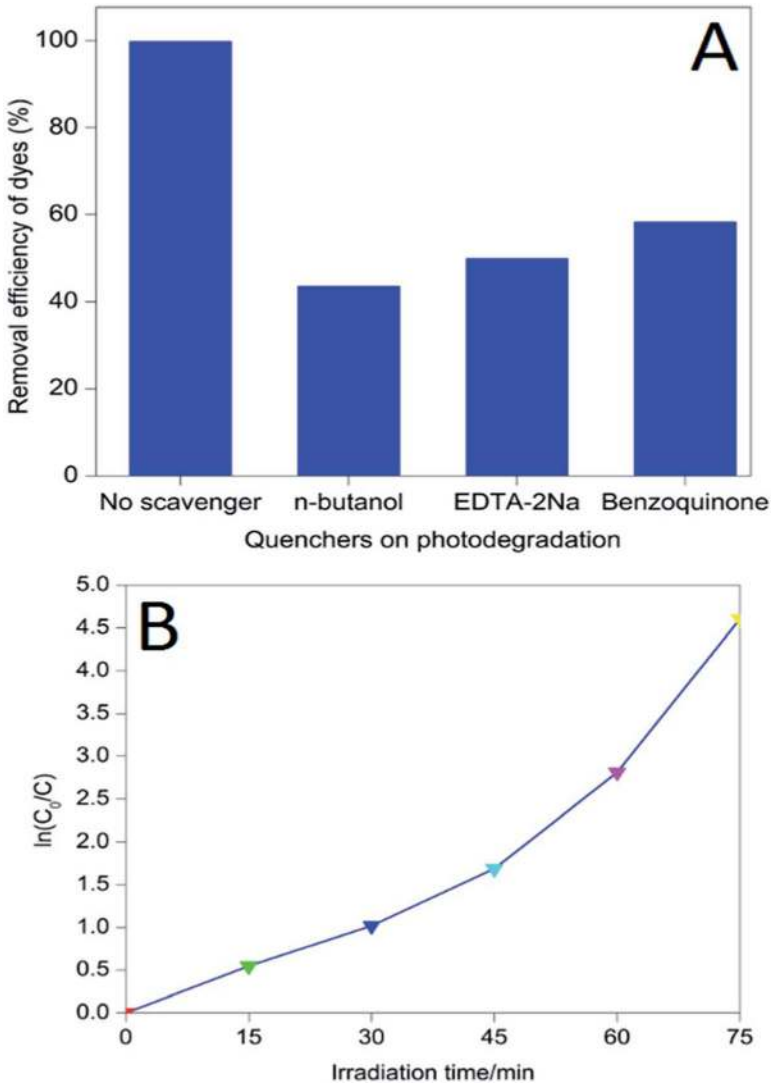

Fig. 15.

(A) Effects of quenchers on photodegradation (B) plot of $\ln(C_0/C)$ *vs.* irradiation time.

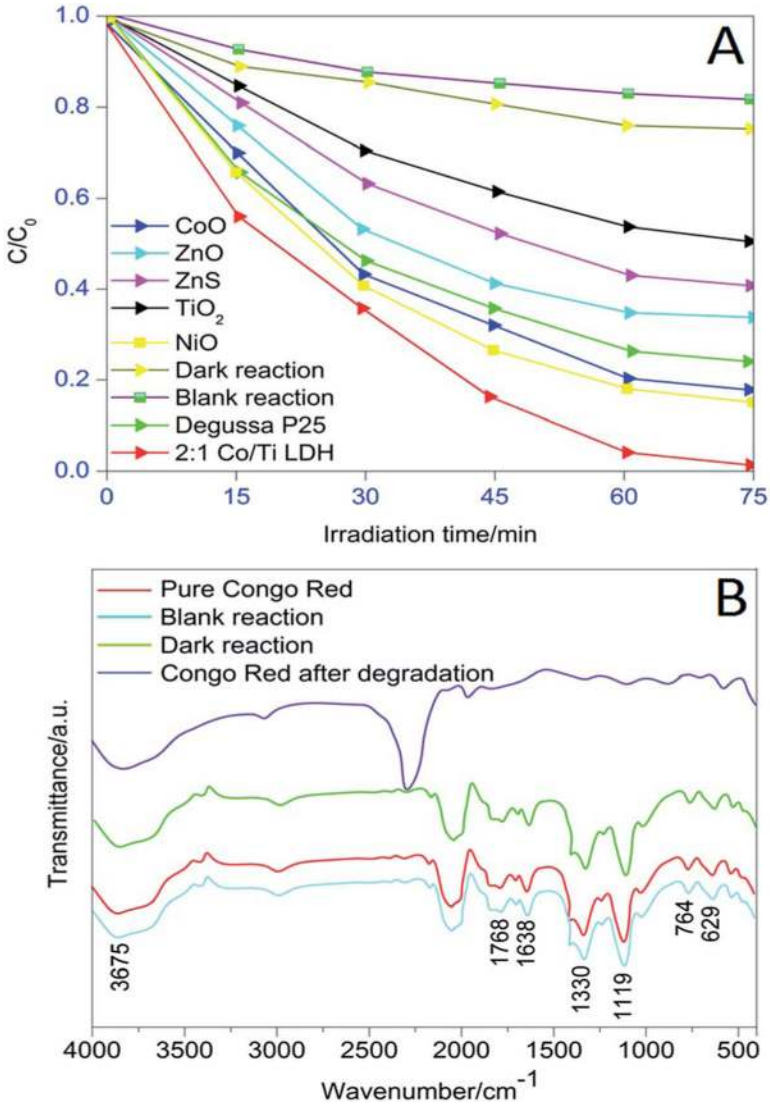

Fig. 16.

(A) Comparative photodegradation of aqueous Congo Red with Co/Ti LDH and commercial photocatalysts, (B) comparative FT-IR analysis of the end products of photodegradation of CR.

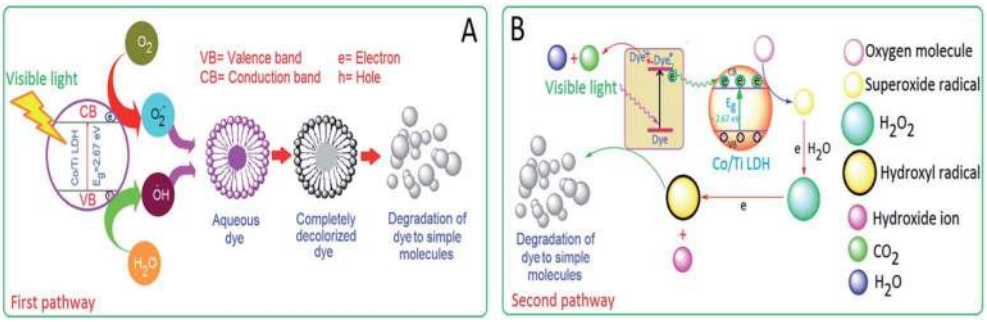

Fig. 17.

Schematic illustrations of mechanistic pathways of photodegradation of CR by 2 : 1 Co/Ti LDH (A) by electron-hole hopping conduction model and (B) by photosensitization of the dye in presence of reactive species.

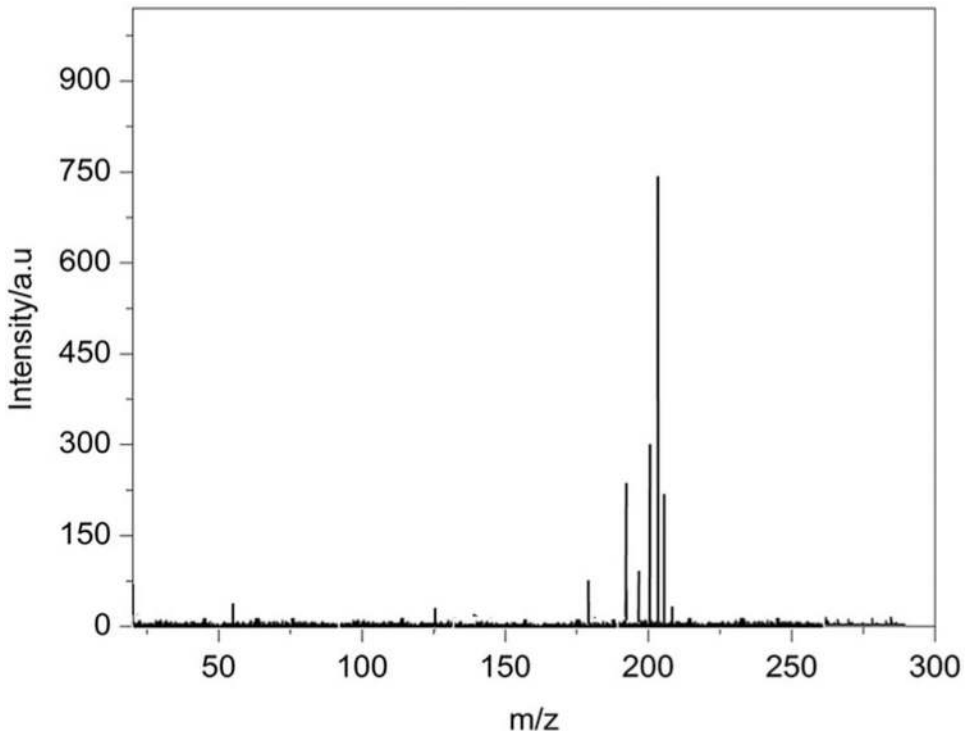

Fig. 18.
Mass spectra of the metabolite of Congo Red.

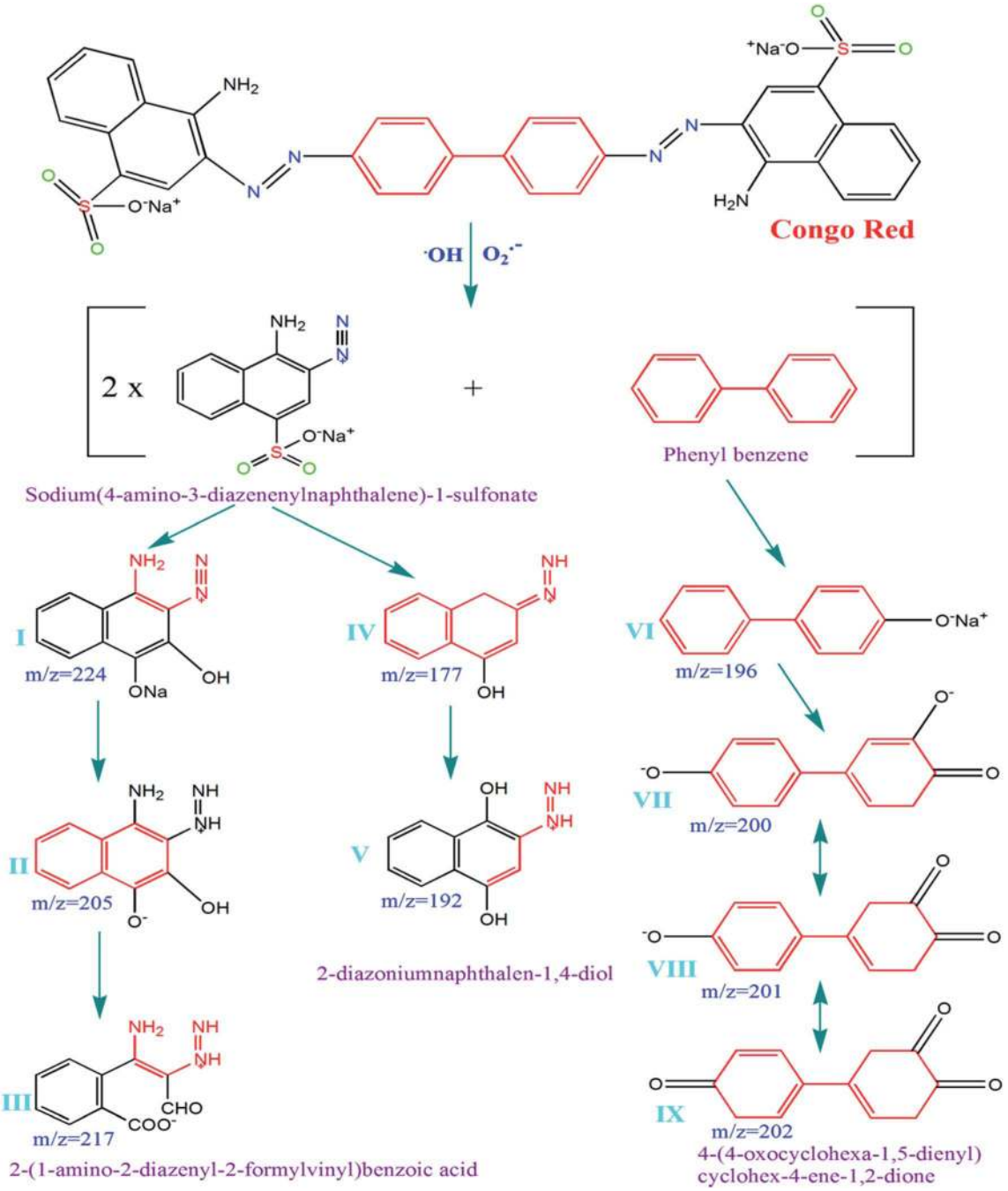

Fig. 19.
Proposed mechanism of photodegradation of Congo Red by 2 : 1 Co/Ti LDH.

Table 1

EDX elemental composition of 2 : 1 Co/Ti LDH

Elements	Weight%	Atomic%	Co/Ti ratio
C K	1.63	1.28	2.03 : 1
N K	4.35	3.15	
O K	12.14	10.21	
Cl K	3.73	1.27	
Co K	52.36	56.34	
Ti K	25.79	27.75	
Total	100.00	100.00	